Rotman Lens Design and Simulation in ISM's Band

Mohammed Khalid Ibraheem Al-obaidi

Submitted to the
Institute of Graduate Studies and Research
in partial fulfillment of the requirements for the Degree of

Master of Science
in
Electrical and Electronic Engineering

Eastern Mediterranean University
August 2014

Gazimağusa, North Cyprus

Approval of the Institute of Graduate Studies and Research

Prof. Dr. Elvan Yılmaz
Director

I certify that this thesis satisfies the requirements as a thesis for the degree of Master of Science in Electrical and Electronic Engineering.

Assoc.Prof. Dr. Hasan Demirel
Chair, Department of Electrical and Electronic Engineering

We certify that we have read this thesis and that in our opinion it is fully adequate in scope and quality as a thesis for the degree of Master of Science in Electrical and Electronic Engineering.

Assist. Prof. Dr. Rasime Uyguroğlu
Supervisor

Examining Committee

1. Prof. Dr. Hasan Amca
2. Assoc. Prof. Dr. Hasan Demirel
3. Asst. Prof. Dr. Rasime Uyguroğlu

ABSTRACT

Wide coverage area is one of the most important requirements of the antenna applications, such as radar systems or satellite communications. Rotman lens is a low cost beam forming system that provides wide scan angle and it is simple to implement in microstrip model [1].

Rotman lens is a multi-input device which controls the beam scan angle depending on the phase shift corresponding to the path length between the input source positions and the radiator elements.

In this study, beside the Rotman lens design and implementation, the conventional matching method (taper line) between the lens region and feeder lines was simulated by FEKO [2] [3].

A new matching method based on the transmission line theory was developed by making use of the standing wave pattern obtained from the FEKO simulation results, to match the feeder line to the lens by considering the lens as a parallel plate region with a given aperture width.

Keywords: Rotman lens, steering beam, phased array antenna.

ÖZ

Geniş kapsama alanı, radar veya uydu haberleşme sistemleri gibi anten uygulamalarında çok aranan bir özelliktir. Mikroşerit modele haiz, düşük maliyetli Rotman lens antenler kullanılarak değişik yönlerde hüzme elde edilebilir [1].

Rotman Lens, çok girişli bir yapıya sahip olduğundan, gişiş ve çıkış noktaları arasında dalganın değişik yollar takip etmesinden kaynaklanan faz farkından ötürü, hüzmenin yönü kontrol edilebilir.

Bu çalışmada, literatürdeki Rotman lens tasarımları göz önünde tutulmuş, FEKO benzetim yazılımı uygulanarak, elde edilen sonuçlarların yayınlanan sonuçlarla uyum içerisinde olduğu görülmüştür [2], [3].

Bu çalışmada, 2.45 GHz frekansında çalışan bir Rotman lens tasarımı göz önünde tutulmuş ve Rotman lens ile mikroşerit uyumlaştırması için yöntem geliştirilmiştir.

Paralel iletkenlerden oluşan lens anten ile besleme kablosunu uyumlaştırmak için bir yöntem geliştirilmiştir. Yöntem, FEKO benzetim yazılımı sonuçlarından elde edilen durgun dalda grafiği ve iletim hattı teorisine dayandırılarak geliştirilmiştir.

ACKNOWLEDGMENT

I would like to express my special thanks to my supervisor Asst. Prof. Dr. Rasime Uyguroğlu, for her supporting, understanding, patience and the continuous contribution to complete this study. Also I am grateful to the rector of EMU Prof. Dr. Abdullah Y. Öztoprak for his guidance supporting during the research time.

My appreciation goes to all staff in my in department, especially to the department chairman Assoc. Prof. Dr. Hasan Demirel for his advising and assistance during my study in North Cyprus.

Special thanks to my family for their unlimited supporting, encouraging and their patience.

Finally, I cannot forget my friends to thank them after the completion of this work.

TABLE OF CONTENTS

LIST OF TABLES

LIST OF FIGURES

LIST OF SYMBOLS /ABBREVIATIONS

a	Bowtie antenna side length
C	Light speed
d	Distance between antenna elements
D	Directivity
f_1	Focal length
f_2	Non focal length
h	Substrate thickness
L	Taper length
P_{rad}	Total power radiated
$S_{i\,j}$	S-parameter
U	Radiation intensity
V_i^-	Reflected voltage
V_j^+	Incident voltage
Z_0	Characteristic impedance
Z_L	Load impedance
α	Focal angle
β	Focal ratio
ε_r	Relative permittivity
ε_e	Effective relative permittivity
λ	Wave length
λ_g	Wave guide length
Γ	Reflection coefficient
η	antenna efficiency
ψ	Beam scan angle
θ	Beam scan angle
$\Delta\varphi$	Phase shift
BFN	Beam forming network
DBF	Digital beam forming
EMSS-SA	Electromagnetic software and system south Africa

FEKO	Feldberechnung für Körper mit beliebiger Oberfläche (German acronym means field calculations for bodies with arbitrary surface)
FR4	flame retardant (step) 4
ISM	Industrial, scientific and medical
MOM	Method of moments
MLFMM	Multi-level fast multi-pole method
SWP	Standing wave pattern
TTD	True time delay

Chapter 1

INTRODUCTION

1.1 Introduction

The fast developments in communication systems increased the necessity of wide coverage antennas. On the other hand, the wide coverage area increases the cost of the antenna. Therefore, the need of controlling the beam direction becomes much more important [4].

Many techniques like Butler Matrix and Blass Matrix are developed to control the direction of the beam [5] [6] but these systems were expensive, complex and had low performance.

However, Rotman lens is a beam forming device used to form the beams of the phased array elements electronically in different directions. The lens geometry consist of inner arc that guide the energy to radiator elements through the receiver arc and transmission lines [1] [6].

The phase shifting in the lens depends on the path length difference. Therefore, it is simpler and cheaper compared to other beam forming methods [1] [7].

Many applications depends on Rotman lens such as radar systems, imaging systems, collision avoidance alarm systems and it provides a high performance communication link for peer to peer communication system [8].

1.2 Thesis Objectives

One of the objectives of this thesis is to illustrate the beam steering by designing and simulation microstrip lens using FEKO software. Lens with seven input ports and 2.45GHz was considered.

The main objective is to match a 50Ω feeder line to a parallel plate Rotman lens region having low impedance.

1.3 Thesis Contribution

Since the matching method between the feeder lines of the lens and the lens geometry consider an important and practical problem to reduce the energy loss of the source. A new matching method was developed and applied between the lens geometry and feeder line. The results were tested by using FEKO simulation software.

1.4 Thesis Organization

Since, the beam steering depends on the phased array theory; simple example was simulated to describe the concepts of the array theory. The basic fundamental of controlling the scan angle for the phased array is described in Chapter 2, also a brief history of the technical developments of the beam forming, the lens improvements and the applications of the microwave lens are explained in this chapter.

Microwave parameters are revised in Chapter 3. Design equations and lens implementations are discussed in Chapter 4. The validation of FEKO software to

simulate the lens and lens simulation results discussion was also covered in this chapter.

The matching between the lens region and the feeding line is an important factor. The horn tapering model types for matching between feeder lines and the lens region were designed and simulated in Chapter 5.

In Chapter 5, also a new matching method depending on the transition line sections was developed. This method was applied to match a 50Ω line to the low impedance parallel plate region.

Chapter 2

BACKGROUND

2.1 Beam Steering Overview

The flexibility of getting multiple beams in desired directions is an important antenna performance criterion for many radar and communication applications. The electronic scanning devices that depend on producing simultaneous beams in the desired angle have faster scanning ability than the conventional dynamic movement of the antenna aperture.

The beam steering can be defined as controlling of the radiation pattern direction and steer it to the desired angle to attain the coverage of a specific area.

The steering angle of the beam can be controlled by the physical movement of the antenna aperture or by specific techniques that can control the angle of the beam without any movement in the antenna aperture; these techniques are known as the beam forming networks (BFN).

This chapter will cover a brief explanation about the beam steering technique by controlling the phase feeding to the elements and some popular applications.

2.2 Beam Steering Formation

The concept of the steerable pattern is based on controlling the phase of the antenna array elements, so it is important to describe the theory of the antenna array to make the idea more simple and clear.

2.2.1 Antenna Array

An array of antenna is composed of a set of antennas with same specification and same distance between them, designed to operate together to attain a specific radiation pattern [9].

There are two ways to feed array elements depending on the application of array antenna. The elements may be fed by identical power and phase to achieve higher gain with narrower beam width, or by adjusting the phase reached to each element to steer the radiation pattern in a certain direction [10].

Although, arrays are used for getting higher gain and more directive beam, they can also be used for a beam steering. Array of antenna fed by different phase is called phased array antenna. The phase array antenna has many advantages than array antenna. The significant advantage is the ability to steer the radiation pattern to a certain angle without any physical movement in the antenna aperture as shown in Figure 2.3.

There are many techniques to adjust the phase which feed the antenna array. However, they can be classified as active phase shifter or passive phase shifter. Each technique has some advantages and disadvantages, which will be explained in the next sections.

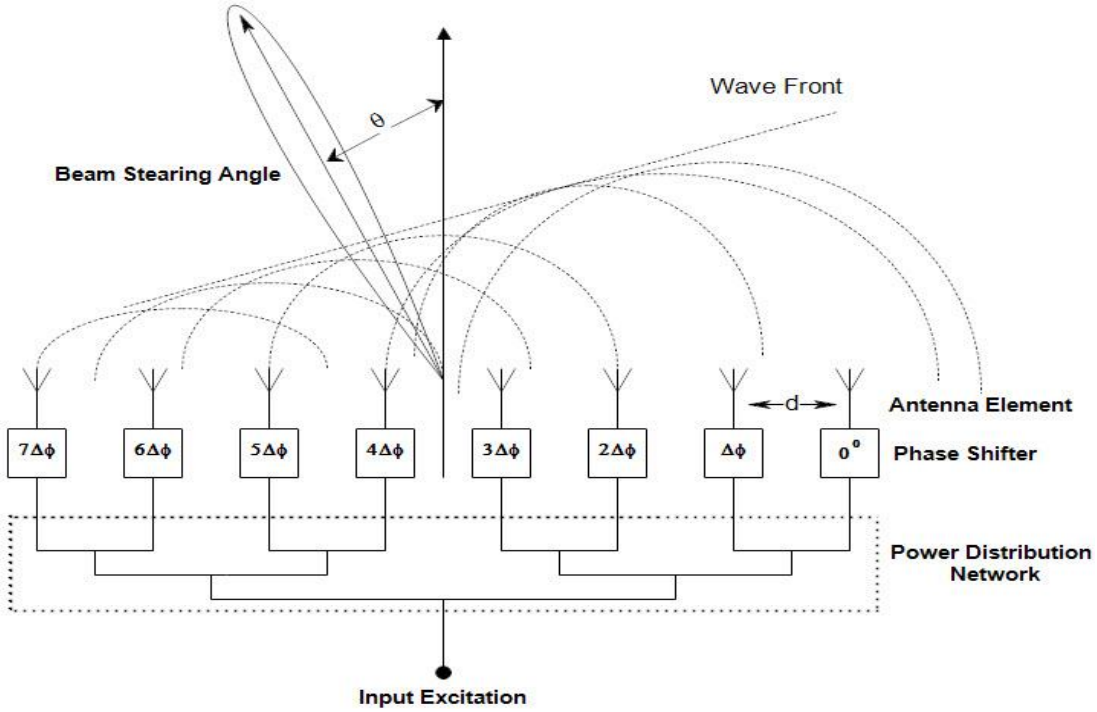

Figure 2.1: Phase shifting and beam steerable direction [4]

For a steering array, with steering angle θ, the phase shift $\Delta\varphi$ and the wave length λ is given by the Equation (2.1):

$$\Delta\varphi = \frac{2\pi * d * \sin\theta}{\lambda} \tag{2.1}$$

The variable d is the distance between the elements and it must satisfy the following condition to decrease grating lobe as it is described in Chapter 3 [4]. Where θ_{max} is the maximum scan angle.

$$\frac{d}{\lambda} = \frac{1}{1+\sin\left|\theta_{\max}\right|} \tag{2.2}$$

To be able to explain the beam steering concept, a simulation of the dipole has been carried out by using the FEKO simulator. Since, the dipole antenna is the simplest antenna [9] and radiates the power evenly in all directions as shown in Figure 2.2 and Figure 2.3.

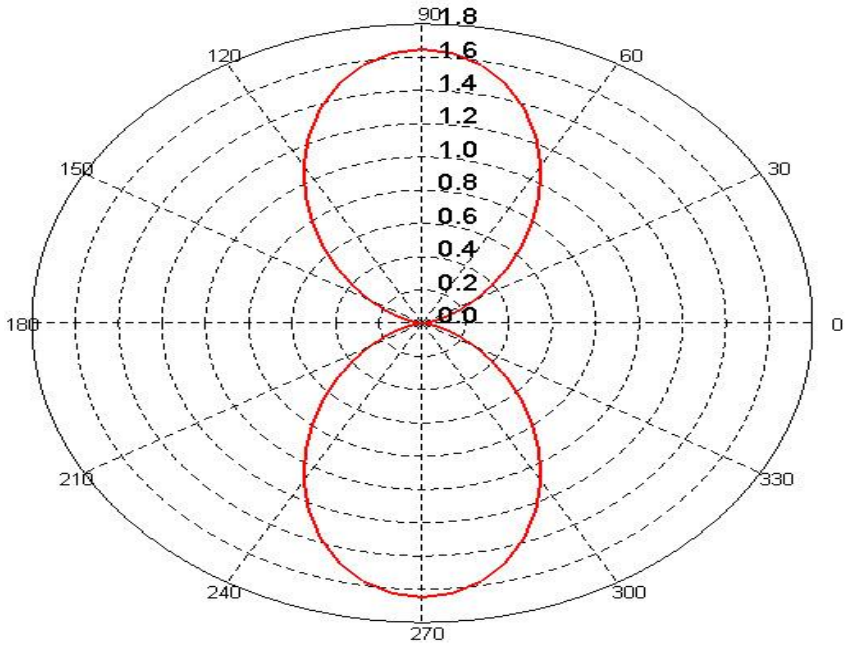

Figure 2.2: The far field of the dipole antenna using polar plot

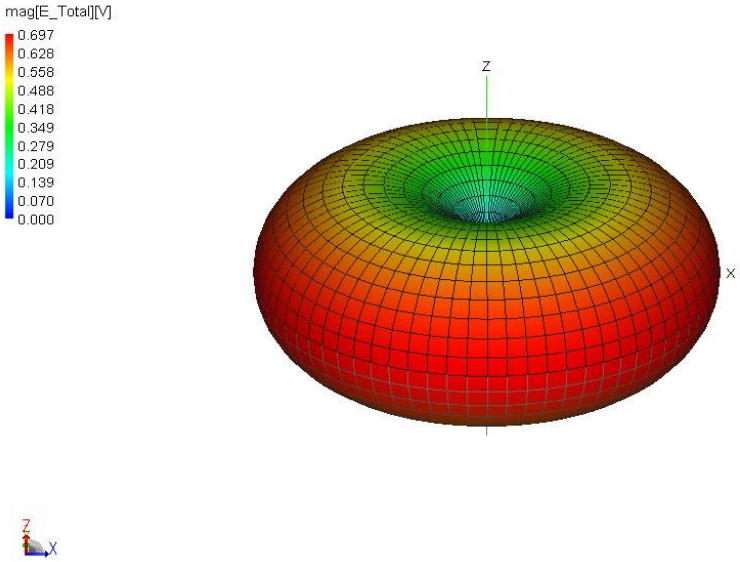

Figure 2.3: Three dimensional far field for the dipole antenna

Then, a six dipole elements array antenna is considered. Each antenna element has 0.5λ length. The elements are z-directed and placed along the x-axis with a separation of 0.5λ. Figure 2.4 and Figure 2.5 demonstrate the results of the elements fed with the same phase i.e. $\Delta\varphi$=0.

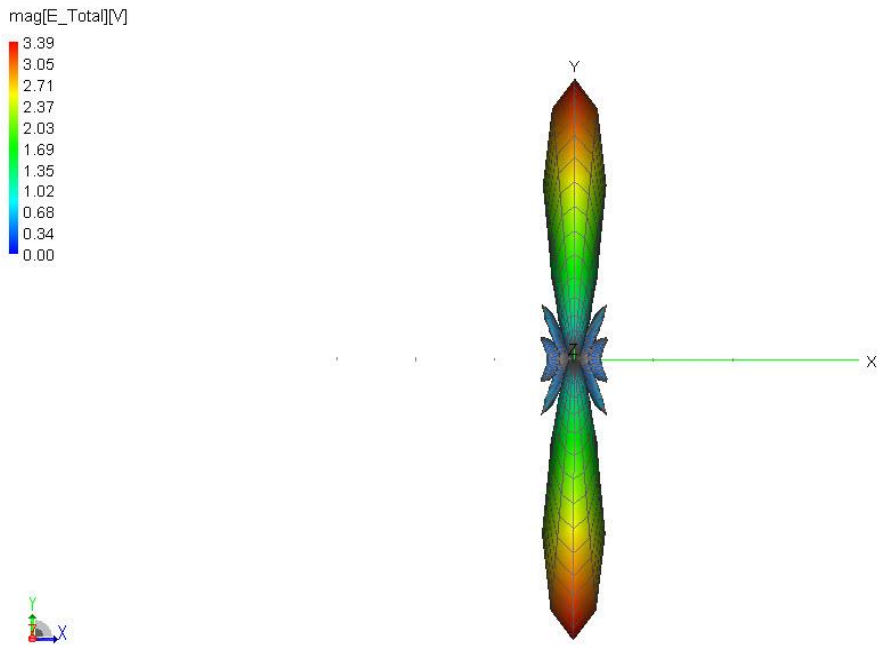

Figure 2.4: 3-D Far field radiation Pattern for the array dipole antenna with Δφ=0

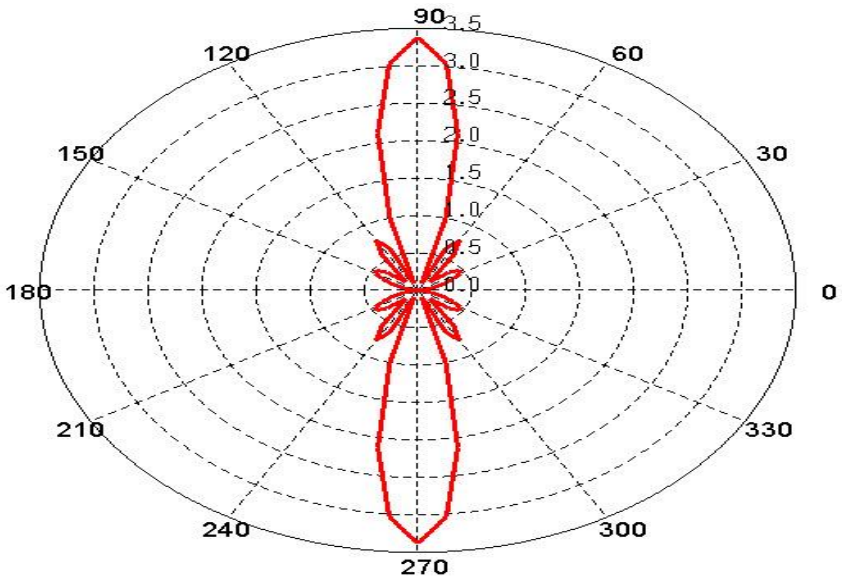

Figure 2.5: Far field radiation pattern for array dipole antenna with $\Delta\varphi$=0

It can be realized from Figure 2.5 that the radiation pattern of the six array elements is narrower than the single element dipole with higher gain as compared to the result demonstrated by Figure 2.2.

Then a 90° phase shift is applied between the feeding elements. The simulated results are shown in Figure 2.6 and Figure 2.7.

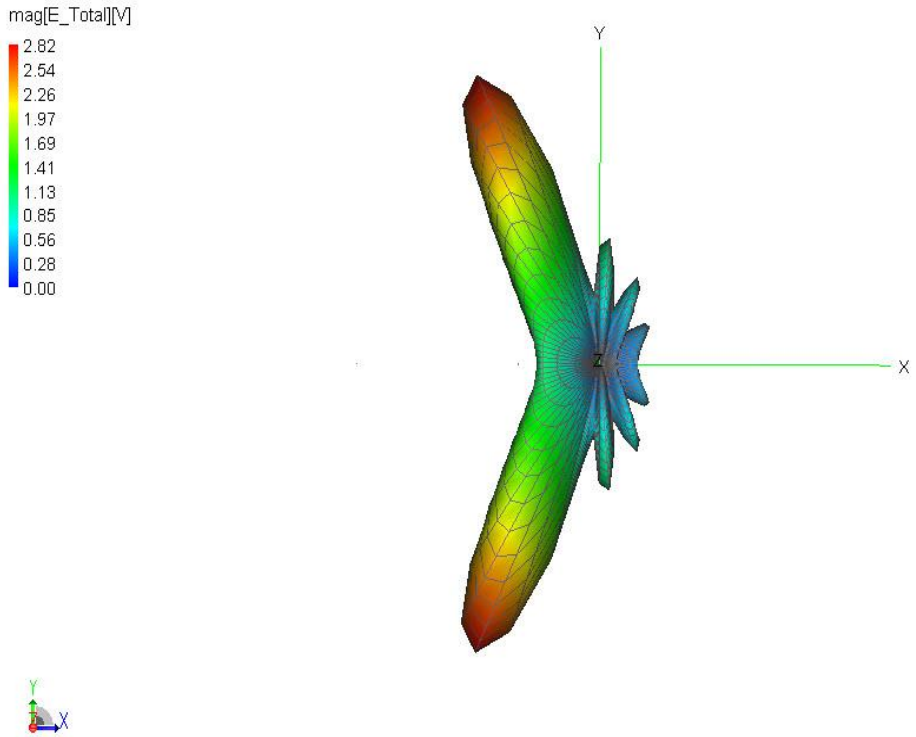

Figure 2.6: 3-D Far field radiation Pattern for array dipole antenna $\Delta\varphi$= 90˚

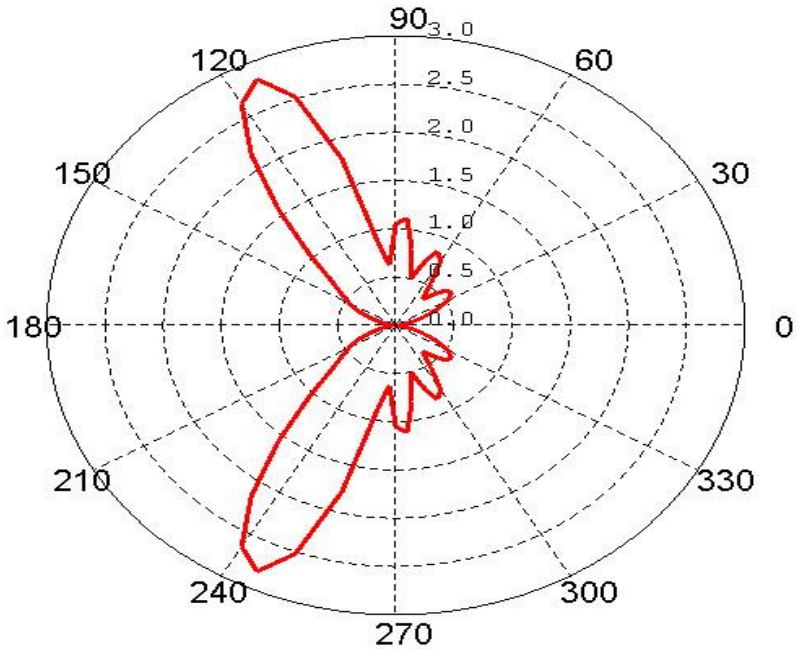

Figure 2.7: Far field radiation pattern for array dipole antenna $\Delta\varphi$= 90˚

The beam steering is implemented by applying progressive phase difference $\Delta\varphi$=90˚, however the last two results demonstrated that there is a significant decrease in the gain and also the side lobe amplitude in the radiation pattern was increased.

2.3 Beam Forming Techniques Overview

Since, in practice, a single excitation with a single phase is available, researchers made many efforts to find ways to obtain a linear progressive phase shift from this excitation for attaining steerable pattern. There are many types of beam forming techniques that can be classified in two categories as analog and digital [4] [10].

In general, beam forming network in a transmit mode delivers the power to the radiation elements with a specific combination of phase to form the final beam, while in a receive mode beam forming combine all the signal from the radiating elements and generate a received signal as shown in the Figure 2.8.

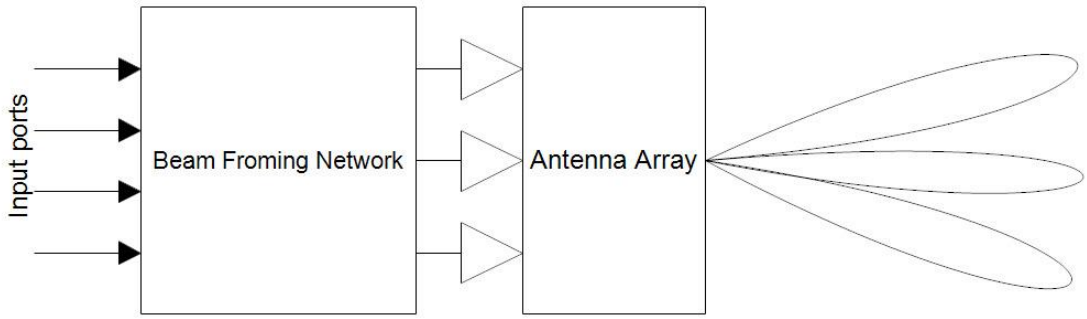

Figure 2.8: Block Diagram of Beam-Forming

The Digital beam forming (DBF) controls the beam direction by using programmable electronic chip [11] as shown in Figure 2.9. The advantages and disadvantages of this type listed in Table 2.1.

Table 2.1: DBF advantages and disadvantages

Advantages	**Disadvantages**
Zero phase error	High cost
Easy to adjust the energy delivered to the antennas	Complexity of system
Flexibility to apply accurate Scanning steps	Limited to low bandwidth application

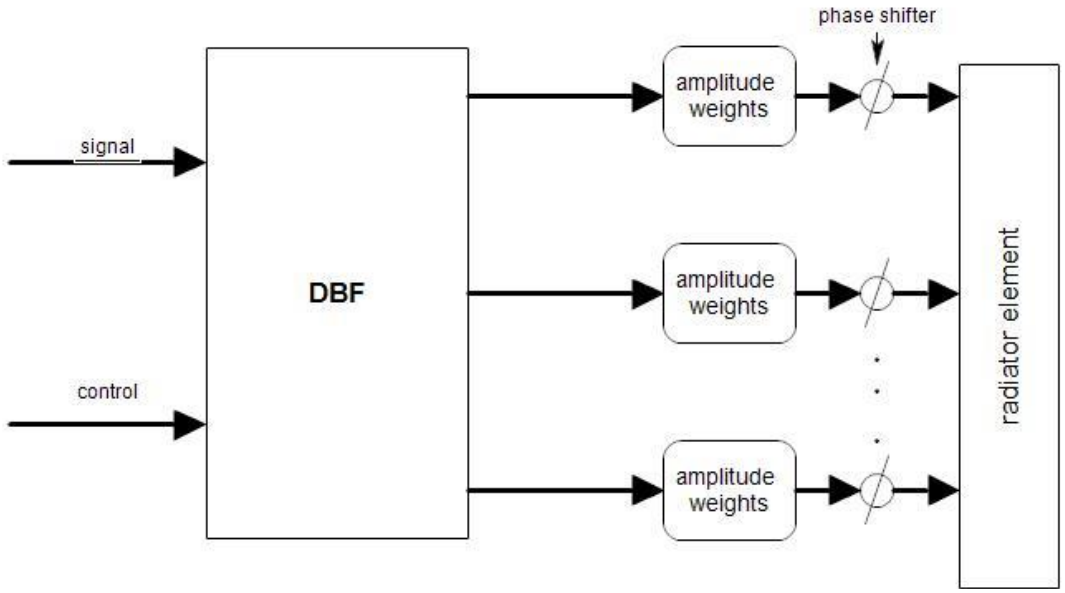

Figure 2.9: Digital Beam Forming system

2.3.1 Array Beam Forming Network

It is considered as an analog BFN. The low cost and less complexity are the significant advantages of this BFN technique. The next section will cover two types of popular types of BFN Blass matrix and Butler matrix.

2.3.1.1 Blass Matrix

Blass matrix is a phase array antenna fed by serial coupled transmission line [5]. Directional couplers distance between transmission line control the phase steering angle as shown in Figure 2.10. Every feed line is designed to produce a specific phase shift to steer the radiation pattern in a certain direction by setting the ratio of the directional coupler. However, the uses of these couplers are considered as a disadvantage of this method because each coupler has specific weight, so it will be costly and a challenge with many couplers in the large matrix design.

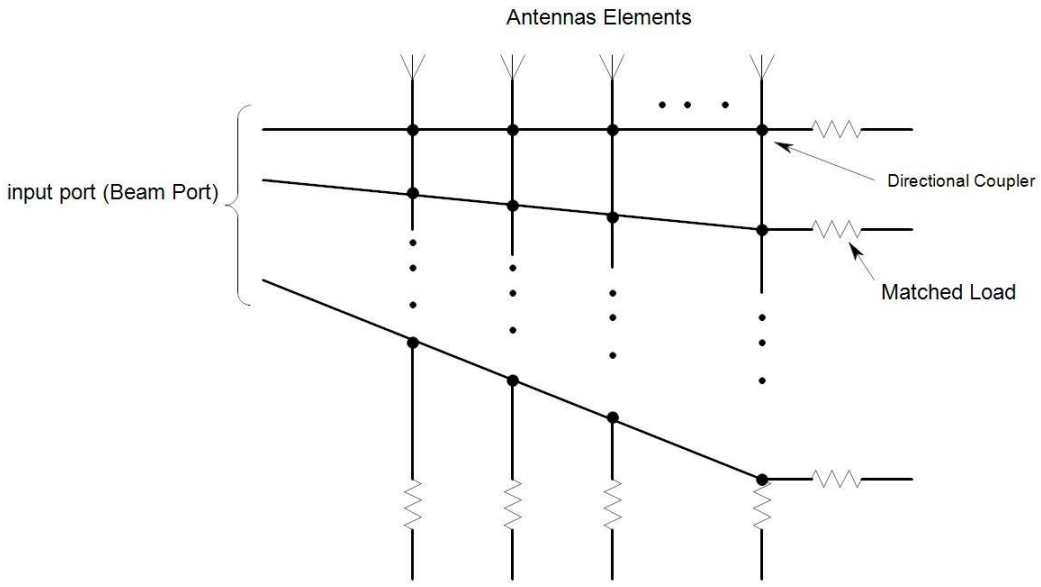

Figure 2.10: Blass matrix diagram [11]

2.3.1.2 Butler Matrix

Similar to the Blass Matrix, Butler Marix is a BFN. The beam steering is controlled by using hybrid power couplers and constant phase shift shown by Figure 2.11. Hybrid power coupler is a junction with two input ports and two output ports used to split the input signal to the two signals having a 90° phase different.

The simple implementation using microstrip and strip line considers as significant advantage of Butler Matrix. However, the beam steering depend on the frequency variation can be considered as a significant disadvantage of this method [6].

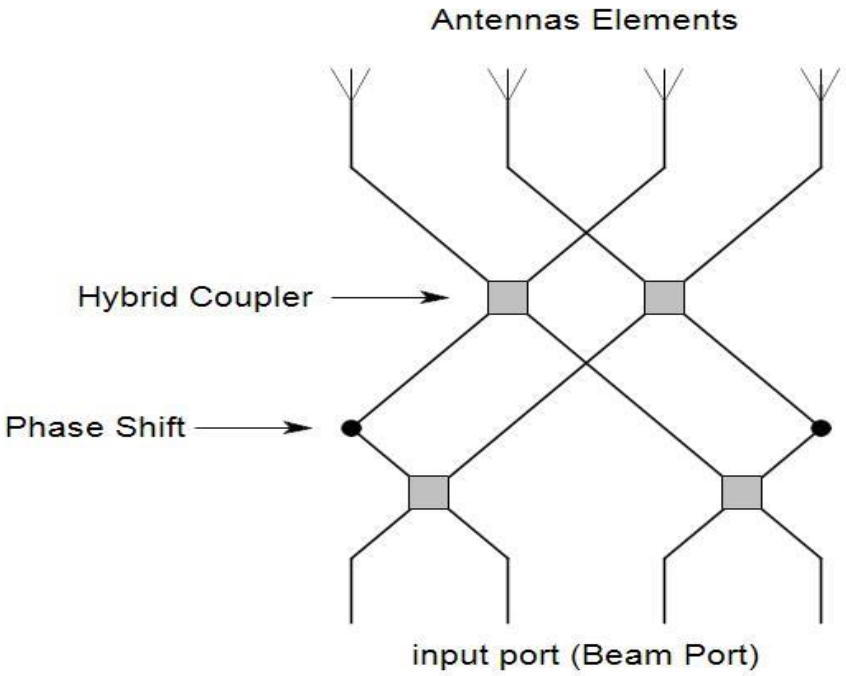

Figure 2.11: Four ports Butler matrix [11]

2.3.2 Lens Beam Forming

Previous sections covered several techniques used for beam forming. Due to the importance of the techniques that depends on controlling the beam direction; many researches and studies are made for improvement.

Microwave lens also can be used as BFN. The phase shift in lens is controlled by the path delay without using any directional coupler and fixed phase shift. The path length difference also called a "true time delay" [1] [12] (TTD) considers the distance between the source and antennas to set the phase reached every element in the array. The difference in this phase will steer the pattern in a different directions.

Lens consists of two arcs and transmission lines guide the energy from these two arcs to the radiation element as shown by Figure 2.12. The position of beam ports (input ports), array ports and the length of transmission lines set the phase reach to each antenna element.

Less complexity, wide bandwidth range, the phase shift independent of frequency, easy of fabrication to microstrip line or strip line can be considered as advantages of using the lens as a beam forming system.

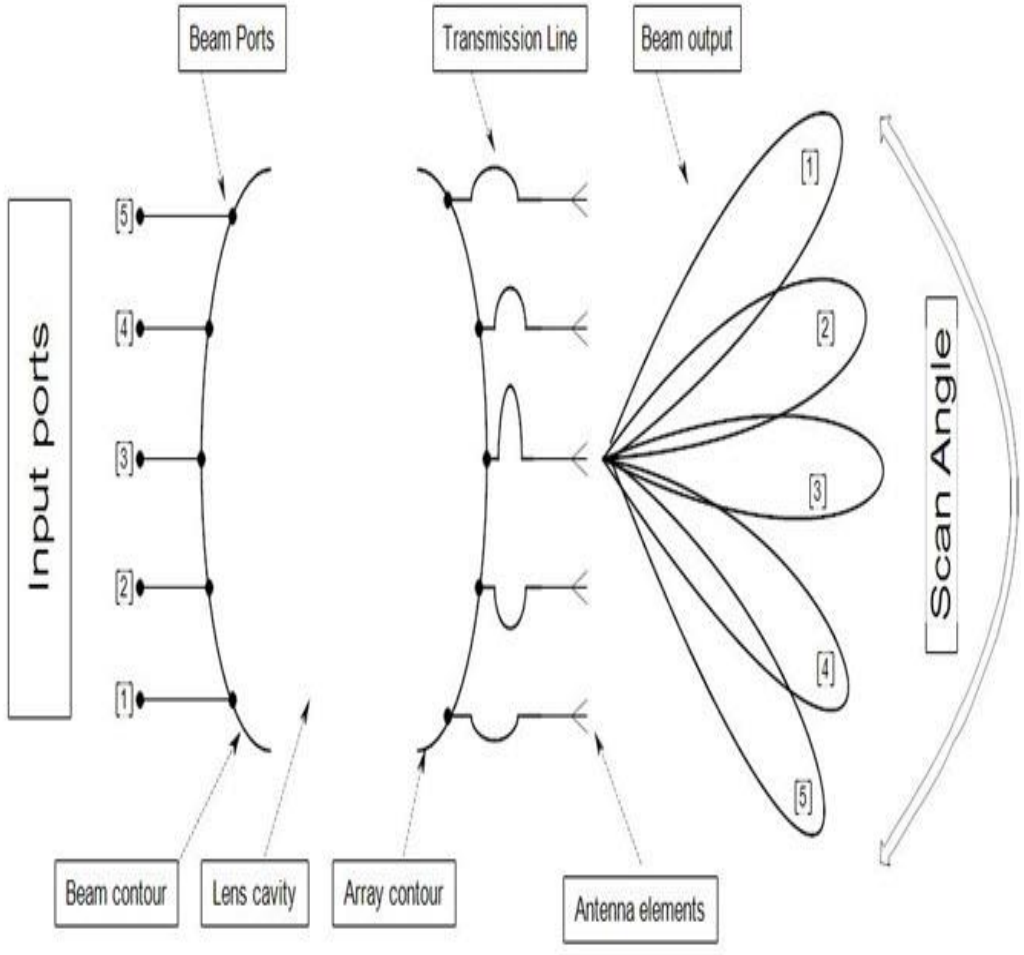

Figure 2.12: Diagram of microwave lens beam forming

There are several scenarios to apply to the geometry of the lens. Also the lens cavity medium can be homogeneous or inhomogeneous. Next sections will cover a summary of lens improvements and its applications.

2.3.3 Summarized History of a Lens as a Beam Forming

A lens has been used in many applications. In general microwave lens are defined as a device that can guide the energy from input ports to the antenna element with adjustment of phase and amplitude. Since 1950 Ruze lens considers the earlier design using parallel plate and constrained line [12]. The R-2R lens mechanism was considered with a ring array design [13]. Gent lens or bootlace lens invented by H. Gent in 1956 as explained in Figure 2.13 and it is used as microwave landing system 1970 [14] [15]. Great phase error improvement and also more freedom in the design variables of the original Ruze lens reported by W. Rotman and R. Turner with three perfect focal points lens [1] as illustrated in Figure 2.14.

In many applications, the need to cover large area of scan angle with less space between the beams, encourage the scientists to meet these requirements by developing the three focal points conventional lens to the four focal lens and non-focal points lens.

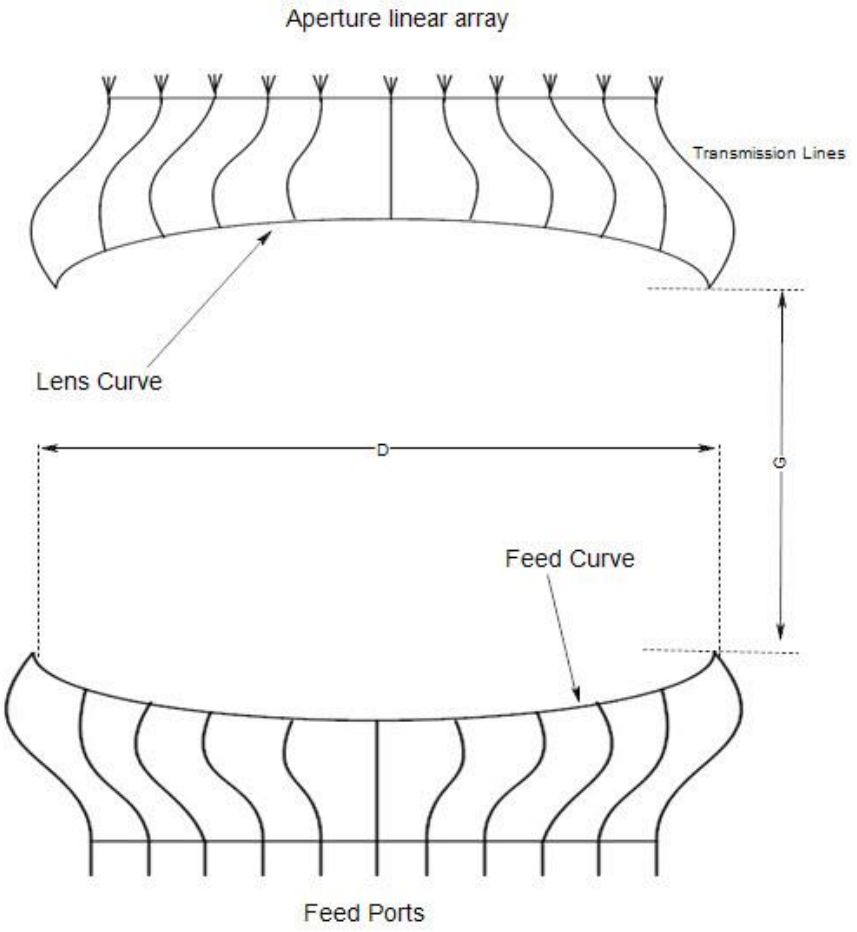

Figure 2.13: Bootlace Lens [14]

The original Rotman lens consists of two parallel plates filled with air as explained in Figure 2.14. The beam contour fed with horn antenna [1]. The transmission line guides the energy between the receiver contour and radiator elements to form the beam.

The beam contour shape is limited with a circular shape and it includes three focal points with zero phase error for the conventional Rotman lens.

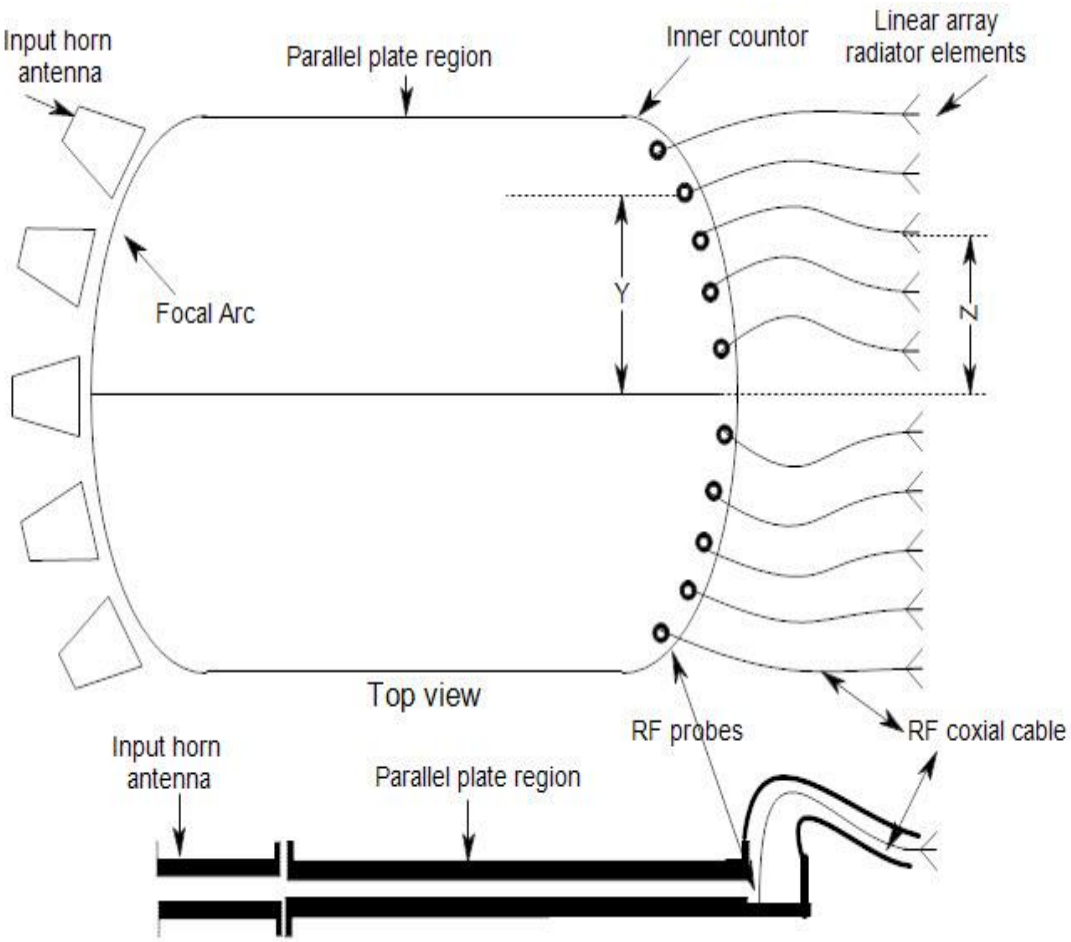

Figure 2.14: The Conventional Rotman lens [1]

Katagi improved the lens design equations to minimize the phase error [7]. To reduce this error Katagi modified the original design equations by changing the circular contour and the radiating angle to yield less phase error.

Then, Hansen redeveloped the seven design variables of the lens geometry to achieve low phase error, low loss and higher degree of freedom. Hansen proposed an elliptical curve as the beam port curve instead of a circular one. The amplitude errors, gain, distance between antennas elements impacts on lens performance were also discussed [16].

After Hansen, Smith found out the relation between the phase orders and lens shape contour. Beside this, he explained the impact of the focal length R on Phase. Study of Smith also includes some calculations the way to minimum lens size with known large array length and scan angle [17].

Another study was done by Smith and Fong to find an amplitude pattern prediction and to determine the performance radiation pattern [18].

Increasing the number of focal point increase the performance ability of scan angle. However, increasing number of beams ports lead to apply beam ports has a phase error in the beam forming non focal points. Three dimension Four focal points is introduced by Jagnmohan B. Original equation design of Rotman lens reformulated to meet the requirements of this lens [19].

Non focal lens points lens and algorithm to reduce the phase error the two dimensions lens are reported by Dong, J., Zaghloul [20].

2.4 Practical Application of Microwave lens

It is desired to have wide coverage area scanning in a certain direction in radar communications system applications. In other words, electronic steerable pattern with large aperture antenna size is very effective for tracking the target quickly without any physical movement in the antenna aperture.

As an example of radar system AN-SLQ-32 electronic defence system [21] [22] with shipboard platform depends on the steerable pattern mechanism using Rotman lens developed by Raytheon Company as shown in Figure 2.15.

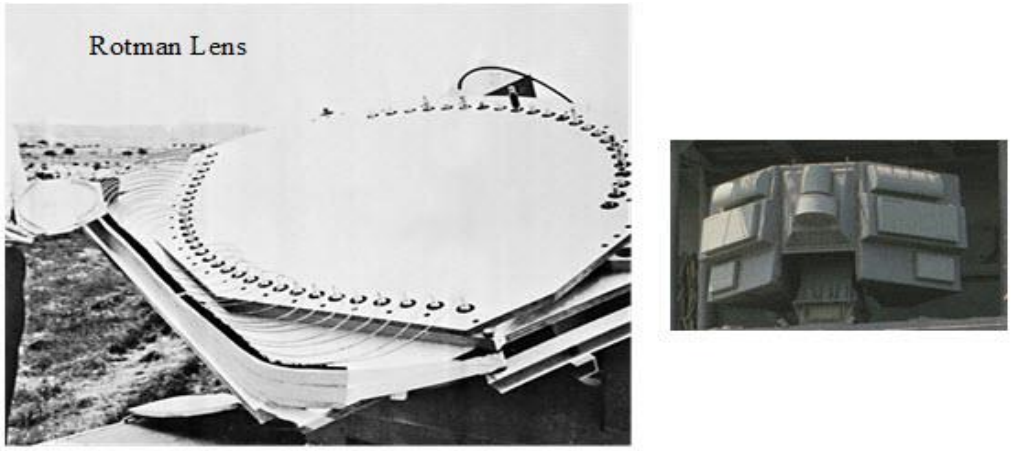

Figure 2.15: AN-SL-32 Radar System [21]

Peer to peer wireless communication system used Rotman lens to direct the beam pattern to the desired angle. Rotman lens used also to guarantee a good performance communication link for a movement platform. Figure 2.16 describes signal tracking between airplane and satellite [23].

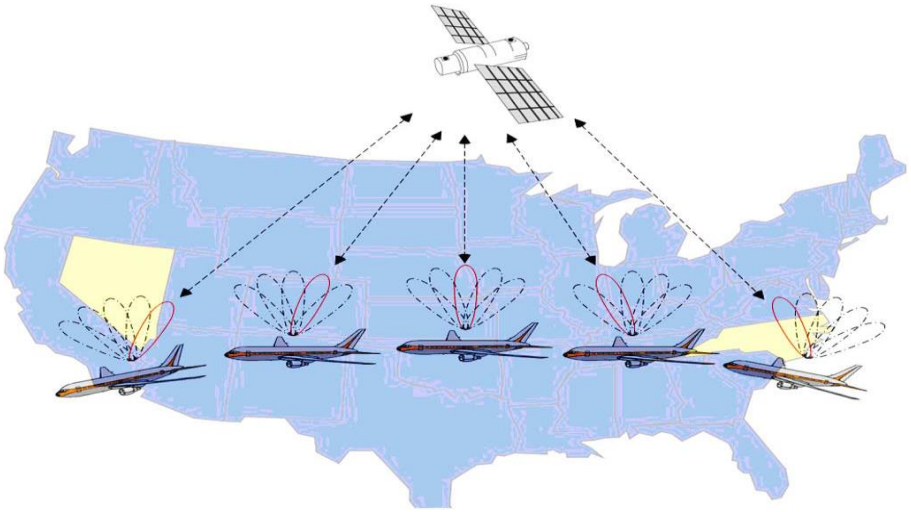

Figure 2.16: Steerable pattern of the communication between airplane and satellite [23]

Smart antenna, imaging system used in biomedical applications, vehicle sensor and earth exploration are applications its system adopted Rotman lens. Figure 2.17 explains compact Rotman lens as a vehicle sensor [24].

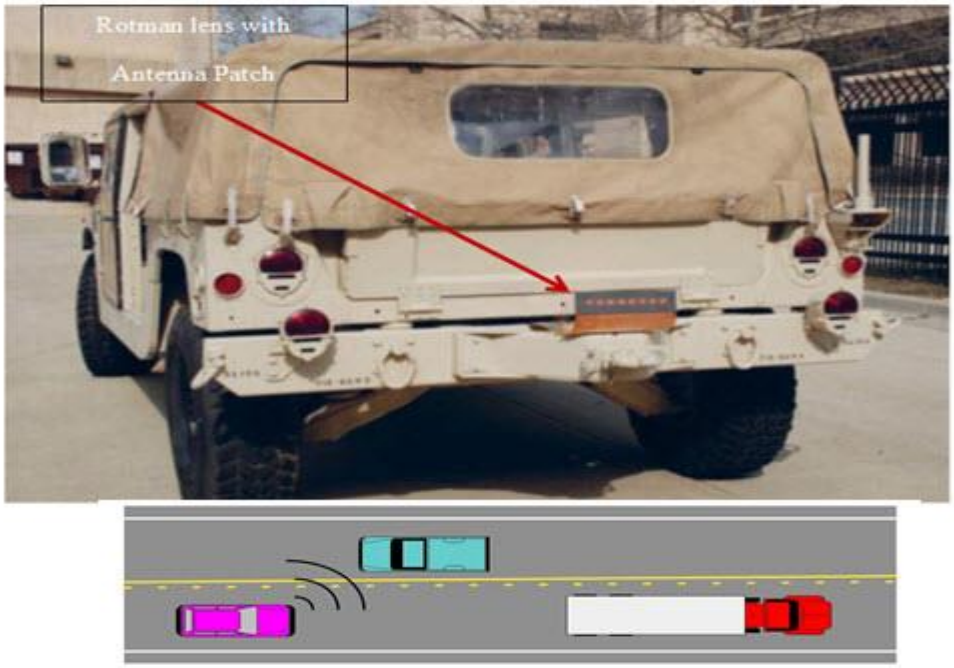

Figure 2.17: Rotman lens as a vehicle sensor [24]

Chapter 3

REVIEW OF MICROWAVE PARAMETERS

3.1 Review of Performance Measurement parameters of Microwave Circuit

The lens beam steering technique is considered a microwave device that controls the direction of the radiation pattern of the phased array antenna which is connected with it. The performance determination of this system is related to the antenna theory and microwave parameters.

FEKO software is an effective simulator with high performance ability to solve the complicated electromagnetic equations. The lens and the phased array element will be simulated by using FEKO software to determine its performance as illustrated in Chapter 4.

In general, the return loss is an important microwave factor to calculate the matching issue. Since the lens is a multiport device, the energy loss between these ports can be calculated by computing the scatter parameters [3].

In the following section some parameters related to microwave circuit theory will be covered to follow the design steps and results explained in Chapter 4.

3.1.1 Frequency Bandwidth

The frequency bandwidth is the range that any radio frequency device can properly. In general the acceptable band is determined when the return loss value is below -10dB. The percentage bandwidth can be determined by using Equation (3.1).

$$\text{Bandwidth} = \frac{f_2 - f_1}{f_c} * 100\% \quad (3.1)$$

Where: f_2, $f1$ are the upper and lower frequencies and f_c is the center frequency as shown by Figure 3.1.

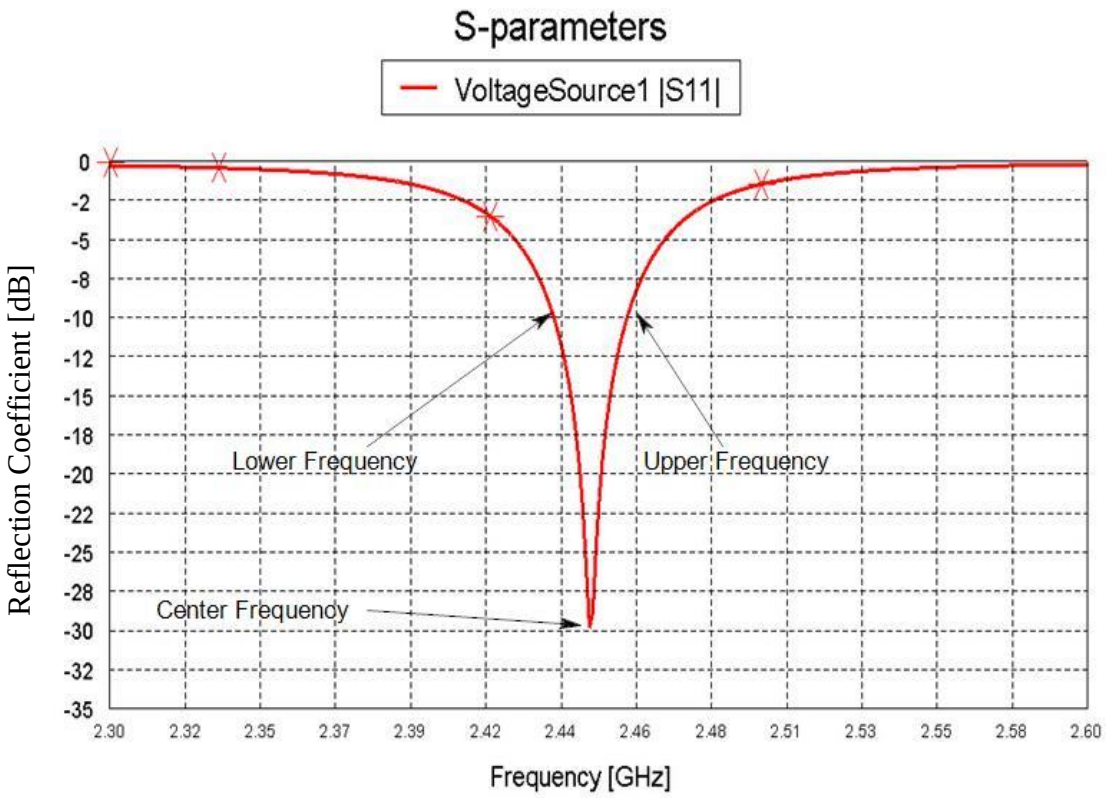

Figure 3.1: Bandwidth explanation

3.1.2 Antenna Radiation Pattern

Graphical explanation used to describe the properties of the radiation around the antenna at a certain position. The radiation can be explained as a function of azimuthal plane and elevation plane.

Radiation pattern appears as lobs. These lobs can be classified into three categories depending on the amount of radiation and its direction. The radiation pattern directed in the desired direction is called the main lob and it is consider as the strongest one. The other two lobs are called as side lobs and back lobs. They are considered as loss and must be a limited magnitude as shown in Figure 3.2.

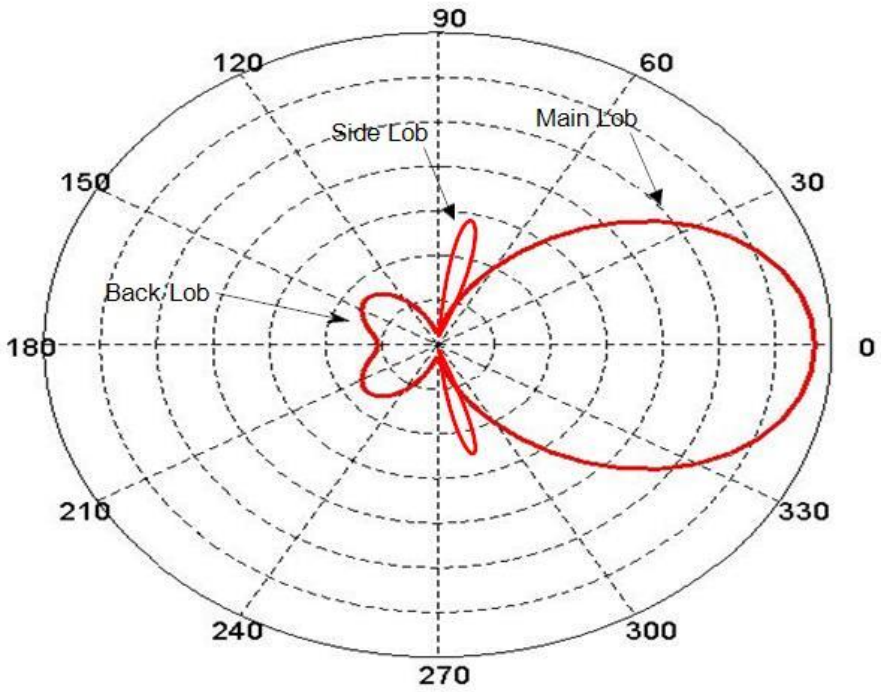

Figure 3.2: Antenna Radiation Pattern

3.1.3 Directivity

It is the measurement of the antenna radiation pattern directionality with recpect to reference antenna (i.e. omnidirectional antenna). Mathematically, Directivity is the ratio between the radiation intensity in a certain direction to the radiation intensity in all directions. It can be calculated by using Equation (3.2) [9].

$$D = 4\pi \frac{U}{P_{rad}} \tag{3.2}$$

Where:

D = Directivity

U = radiation intensity

P_{rad} = total radiated power

3.1.4 Gain

Gain is measurement of the antenna directivity in practice after evaluation of the antenna loss. It can be calculated by using Equation (3.3).

$$\text{Gain} = \eta D \tag{3.3}$$

Where: D is the antenna directivity, η is the antenna efficiency.

It is realized from the Equation (3.3) when the antenna efficiency is equal to 1 (antenna loss equal to zero), the antenna directivity will be equal to the antenna gain.

3.1.5 Scatter Matrix

The beam forming network device may be considered as multi-port radio frequency device as shown in Figure 3.3. The incident and reflected voltages can be determined by calculating the reflection and transmission coefficients S_{ij} which are called scatter parameters.

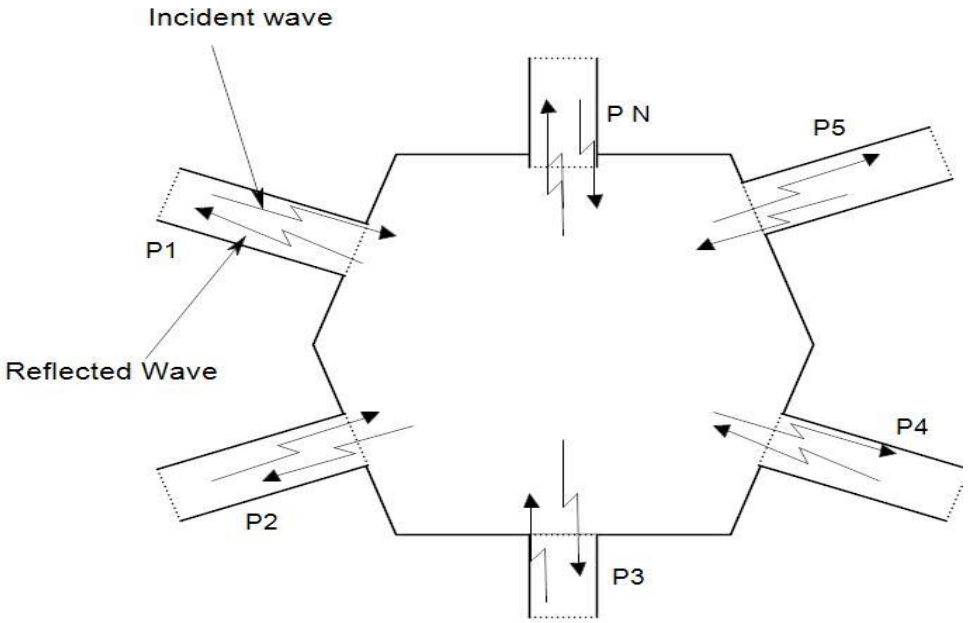

Figure 3.3: Microwave Network [3]

The S_{ii} refers to the reflection coefficient of the ports i and the S_{ij} refers to the transmission coefficient between port i and j when port j is excited. The ratio between the amplitude of reflected voltage V_i^- and the amplitude of incident voltage V_j^+ determine S-parameter as shown in Equation (3.5).

$$S_{ij} = \frac{V_i^-}{V_j^+} \tag{3.5}$$

For N ports microwave network S-parameter can be calculated by using $N \times N$ matrix dimensions [3].

$$\begin{pmatrix} S_{11} & \cdots & S_{1N} \\ \vdots & \ddots & \vdots \\ S_{N1} & \cdots & S_{NN} \end{pmatrix} \begin{pmatrix} V_1^+ \\ \vdots \\ V_N^+ \end{pmatrix} = \begin{pmatrix} V_1^- \\ \vdots \\ V_N^- \end{pmatrix} \tag{3.6}$$

In a microwave network device, during the calculation the of scatter matrix coefficients when a specific port was excited all the others ports must be connected to a match load to prevent the incident reflections inside the network device.

Chapter 4

DESIGN AND SIMULATION RESULT

4.1 Introduction

In this study, a Rotman lens simulation is carried out by using FEKO software. FEKO is a commercial simulation software developed by "EMSS-SA" used for solving electromagnetic problem. It is based on "Method of Moments (MOM)“ and "multi-level fast multipole method (MLFMM)” [25] numerical method. The software also includes optimisation ability by using optimisation function like genetic algorithms.

4.2 Rotman Lens Equation Design and Formulation

Rotman lens consists of two arcs. Input arc includes beam ports and it is known as the beam contour. The second arc is connected between the lens cavity and the array of antenna through transmission lines with length W. This arc is known as the receiver contour.

The lens cavity medium and transmission line can be designed using homogenous or inhomogeneous relative permittivity. This study will cover homogenous medium only [26].

A typical lens is demonstrated by Figure 4.1. The beam port may be considered a known curve (i.e. circular, elliptical) [16] with three focal points F_1, F_2 and F_3. The receiver contour $P(X,Y)$, as well as the transmission line is calculated by using the geometrical optics as explained below as shown in the Equations (4.1)-(4.3) [26] [27].

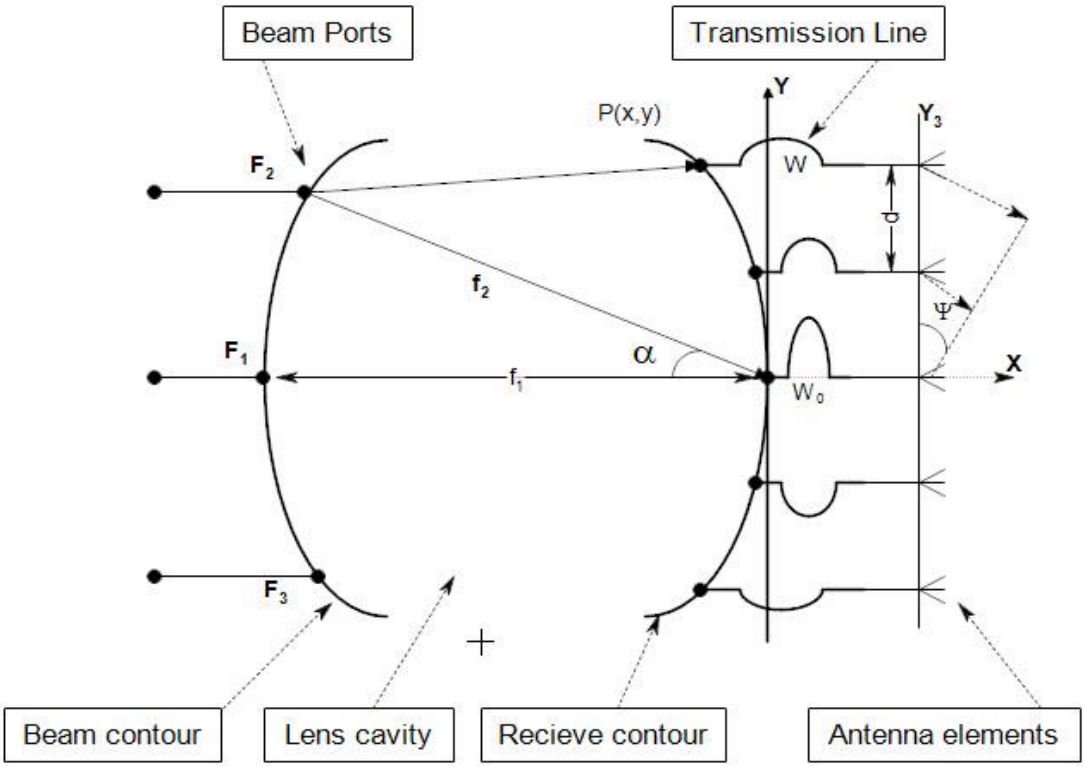

Figure 4.1: Lens design configuration

Each $P(X,Y)$ and W are calculated by equating the path length from F_1, F_2 *and* F_3 focal points to the related phase fronts [1]. The following three equations can be obtained and solved for X, Y and W. Where F_1P, F_2P and F_3P are the distance between F_1, F_2 and F_3 and any point on the receiver counter.

$$\overline{F_1P}\sqrt{\varepsilon_r} + W\sqrt{\varepsilon_e} = f_1\sqrt{\varepsilon_r} + W_0\sqrt{\varepsilon_e} \quad (4.1)$$

$$\overline{F_2P}\sqrt{\varepsilon_r} + W\sqrt{\varepsilon_e} + Y_3\sin\psi = f_2\sqrt{\varepsilon_r} + W_0\sqrt{\varepsilon_e} \quad (4.2)$$

$$\overline{F_3P}\sqrt{\varepsilon_r} + W\sqrt{\varepsilon_e} - Y_3\sin\psi = f_2\sqrt{\varepsilon_r} + W_0\sqrt{\varepsilon_e} \quad (4.3)$$

Where

$$w = \frac{\sqrt{\varepsilon_e}}{\sqrt{\varepsilon_r}}\frac{-b \pm \sqrt{b^2 - 4ac}}{2a} \quad (4.4)$$

$$x = \frac{Y_3^{\,2}\sin^2\psi}{2\varepsilon_r(\beta\cos\alpha - 1)} + \frac{(1-\beta)w}{\beta\cos\alpha - 1}\sqrt{\frac{\varepsilon_e}{\varepsilon_r}} \quad (4.5)$$

$$y = \frac{Y_3\sin\psi}{\sqrt{\varepsilon_r}f_1\sin\alpha}\left(1 - \frac{w}{\beta}\frac{\sqrt{\varepsilon_e}}{\sqrt{\varepsilon_r}}\right) \quad (4.6)$$

and

$$a = 1 - \left(\frac{1-\beta}{1-\beta C}\right)^2 - \frac{\zeta^2}{\beta^2\varepsilon_r} \quad (4.7)$$

$$b = -2 + \frac{2\zeta^2}{\beta\varepsilon_r} + \frac{2(1-\beta)}{1-\beta C} - \frac{\zeta^2 S^2(1-\beta)}{(1-\beta C)^2\varepsilon_r} \quad (4.8)$$

$$c = \left(-\zeta^2 + \frac{\zeta^2 S^2}{1-\beta C} - \frac{\zeta^2 S^2}{1-\beta C} - \frac{\zeta^2 S^4}{4(1-\beta C)}\right)\frac{1}{\varepsilon_r} \quad (4.9)$$

$$\beta = \frac{f_2}{f_1},\ \zeta = \frac{Y_3\sin\psi}{f_1\sin\alpha},\ S = \sin\alpha,\ C = \cos\alpha$$

The variables description of the above equations are explained in Table 4.1.

Table 4.1: Description of the design parameters

Parameters	**Descriptions**
f_1	Focal length
f_2	Non Focal length
α	Focal angle
β	Focal ratio
ε_r	Relative permittivity of lens cavity
ε_e	Relative permittivity of transmission line
w	Transmission line length normalized to f_1
d	Distance between radiator element
Y_3	Radiator element coordinate on Y axis
x, y	Receiver contour coordinate normalized to f_1
ψ	Beam scan angle

The necessary lens dimensions were obtained by using Matlab code to construct the contours of the lens.

The truncation of the lens (i.e. side walls) may cause reflections that reflections reduce the efficiency of the lens. Due to the importance of the reflections many engineers worked to eliminate the side wall effects [28] by connected dummy ports to the side walls as explained in Figure 4.3. Also the tapering techniques are widely used for matching between the 50Ω transmission line and the lens geometry. This topic will be covered in Chapter 5 in details.

4.3 Rotman lens Implementations

This chapter covers a two Rotman lens implementation simulated by FEKO. A lens is adopted with direction arrival estimation system [29]. The consideration for the simulation of this design is the validation of Rotman lens simulation by FEKO software.

4.4 Lens Simulation

Ping's study [29] was taken as reference for validation. The lens design parameters are listed in the Table 4.2.

Table 4.2: Design parameters [29]

No. of beam ports	13	Focal length	4 lambda
No. of antenna ports	6	Displacement distance	0.5 lambda
No. of dummy ports	6	Substrate thickness	1.6 mm
Scan angle	60°	Height	495 mm
Relative permittivity	4.4	Width	335 mm
Loss tangent	0.02	Bandwidth	2-6 GHz

The beam and receiver contour are constructed by Matlab as shown in Figure 4.2.

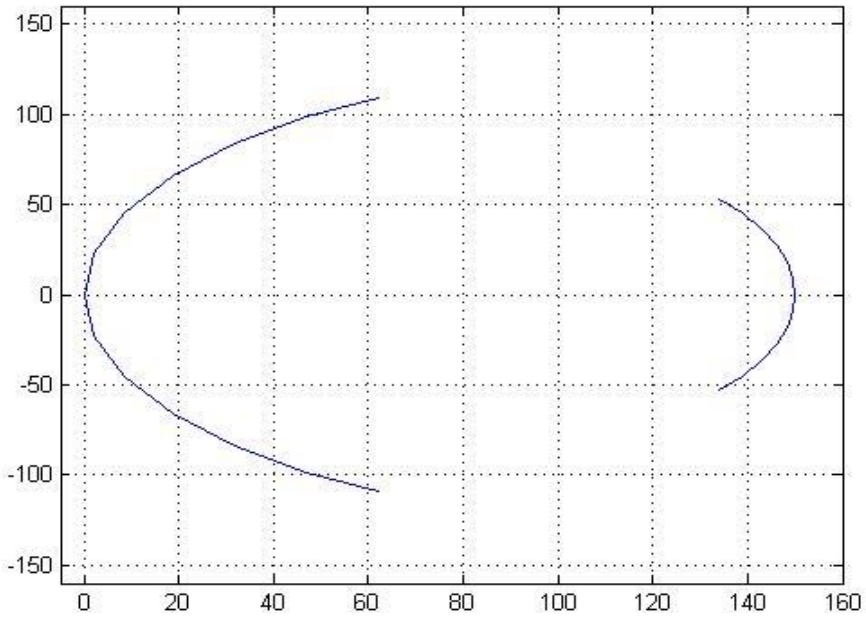

Figure 4.2: Lens contours calculated by Matlab

The lens geometry will be matched to the 50Ω characteristic impedance line through the taper. The width of these transmission lines can be determined by applying the followingequations.

$$\varepsilon_e = \frac{\varepsilon_r + 1}{2} + \frac{\varepsilon_r - 1}{2}\left(\frac{1}{\sqrt{1+12h/w}}\right) \tag{4.10}$$

$$Z_0 = \begin{cases} \dfrac{60}{\sqrt{\varepsilon_e}} \ln\left(\dfrac{8h}{w} + \dfrac{w}{4h}\right) & for\ (w/h) \le 1 \\ \dfrac{120\pi}{\sqrt{\varepsilon_e}\,(w/h + 1.393 + 0.667\ \ln(w/h + 1.444))} & for\ (w/h) \ge 1 \end{cases} \tag{4.11}$$

Where: ε_e is the effective relative permittivity, ε_r is the substrate relative permittivity, h is the substrate thickness, w is the width of the transmission line and Z_0 is the characteristic impedance of the transmission line.

The complete FEKO model design is shown in Figure 4.3 and demonstrates the lens including the side walls and the tapered ports.

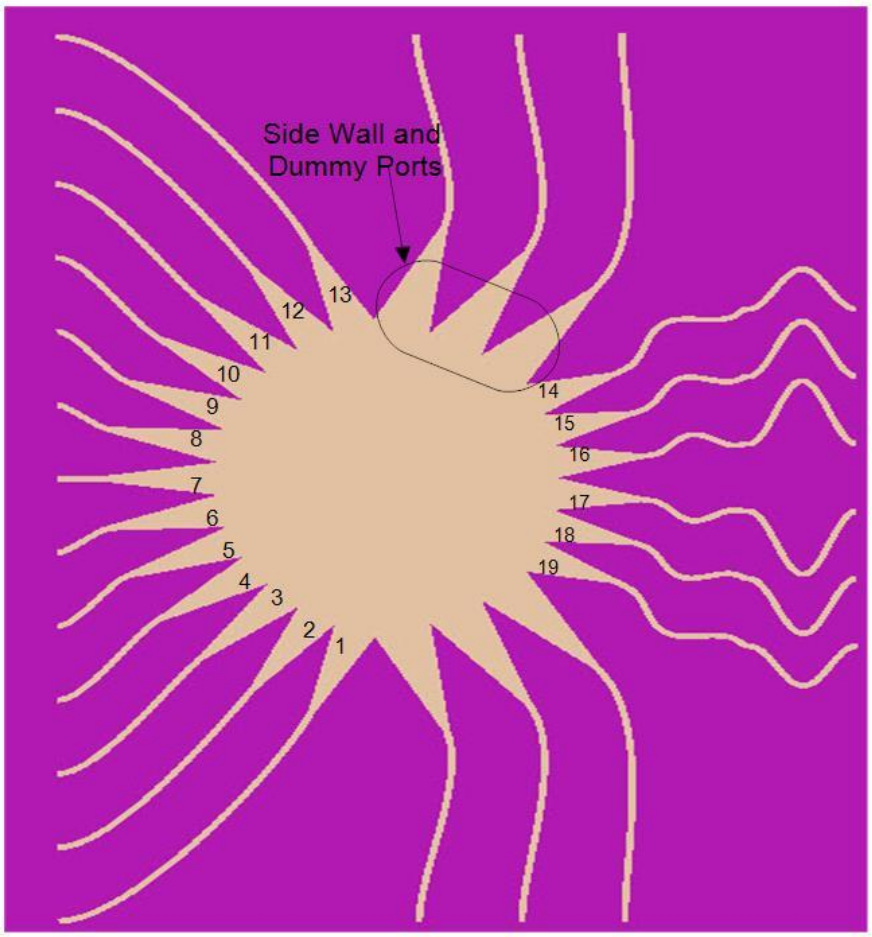

Figure 4.3: Lens FEKO model

The beam ports are numbered from 1-13 and the array ports numbered from 14-19. The other ports are the dummy ports used to reduce the incident reflection inside the lens.

The test is done by applying an excitation at port 7 and recording the transmission coefficients between port 7 and other array ports. The results are shown by Figure 4.4 and Figure 4.5, where Figure 4.4 is the reference result and Figure 4.5 is the FEKO result.

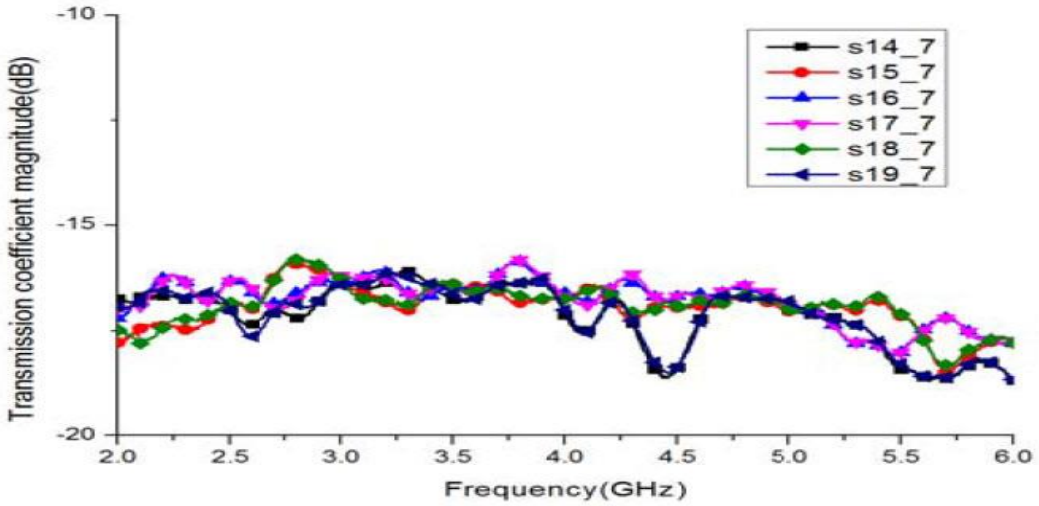

Figure 4.4: Measured transmission coefficients [29]

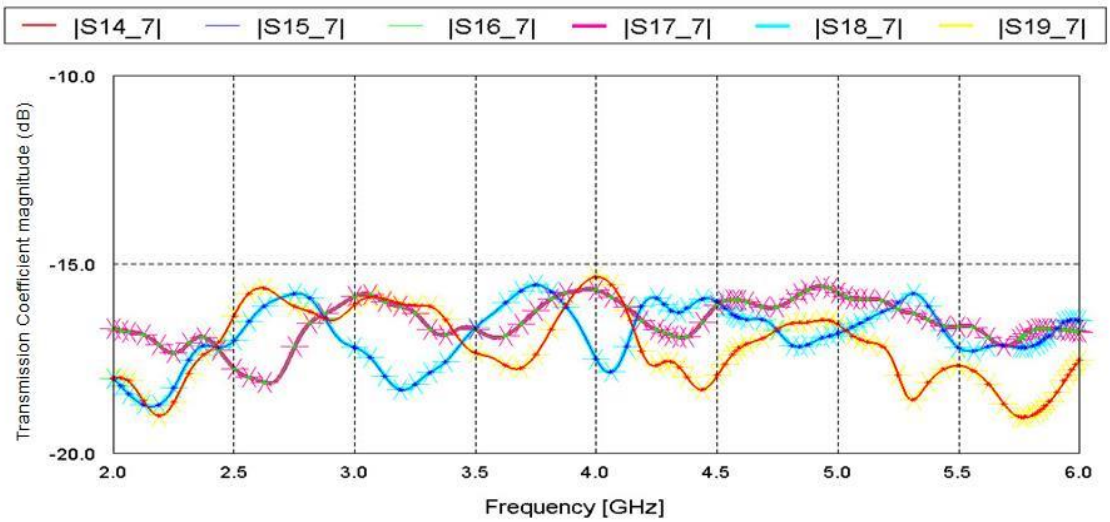

Figure 4.5: Simulated transmission coefficients by FEKO

Due to the symmetrical geometry of the lens, Symmetrical ports have the same energy level. The results show that, the excitation energy from port 7 reached to the

array ports with a little fluctuation about 3dB, approximately around -17dB; this is a good indication of this lens as a beam forming lens.

Since, the lens geometry consider has a large, multiport and complicated structure, also due to the limitation in FEKO hardware platform ability; we will consider smaller lens geometry with less number of ports to discuss all the simulation results with details as the next.

4.5 Lens with ISM's Band

ISM band (Industrial, Scientific and Medical) considering 2.45 GHz has many applications. The lens below is designed to operate at 2.45GHz center frequency. The other relevant design parameters are tabulated by Table 4.3.

Table 4.3: Design parameters

No. of beam ports	7	Focal length	1.5 lambda
No. of antenna ports	4	Displacement distance	0.38 lambda
No. of dummy ports	6	Substrate thickness	1.6 mm
Scan angle	35˚	height	221 mm
Relative permittivity	4.4	Width	238 mm
Loss tangent	0.02	Center frequency	2.45 GHz

The beam and the receiver contours calculated by Matlab are shown in the Figure 4.6.

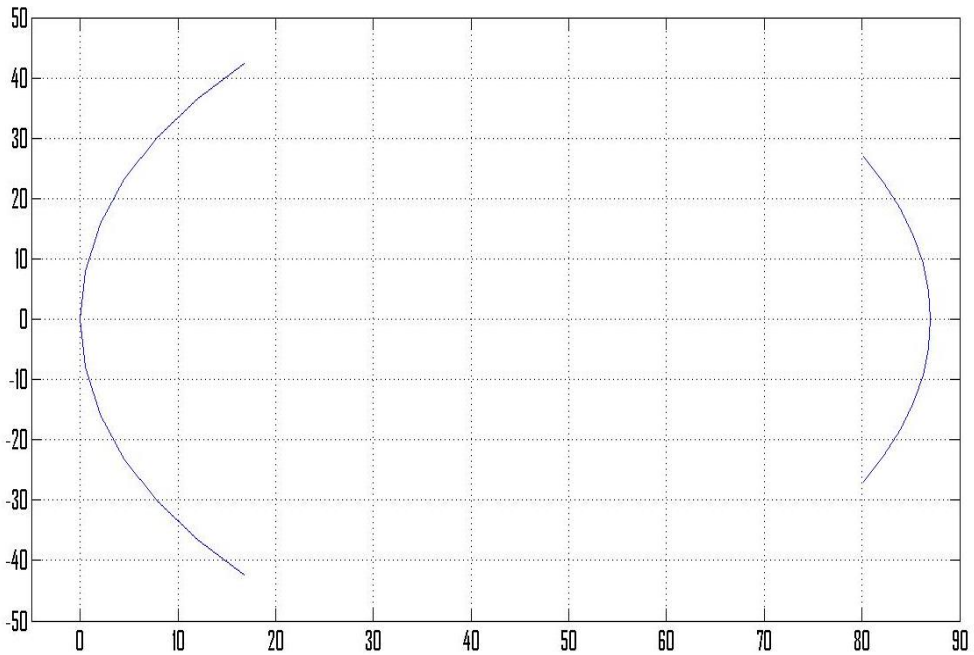

Figure 4.6: Beam and receiver contour calculated by Matlab

The FEKO model of the complete lens geometry is shown in the Figure 4.7.

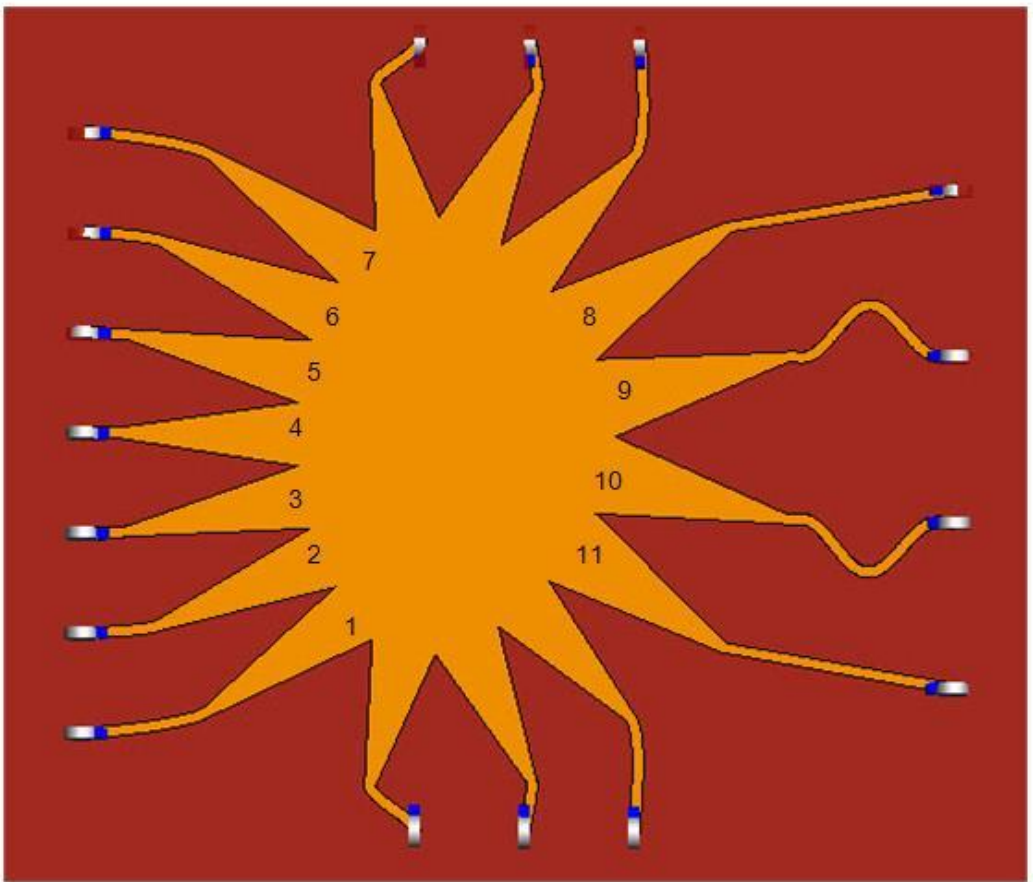

Figure 4.7: FEKO lens model

Figure 4.7 indicates that the beam ports are numbered from 1 to 7 and the array ports from 8 to 11. The other ports are the dummy ports terminated by 50Ω load (matched load) to reduce the reflection inside the lens.

It is important to note that the tapering technique was used for matching. The design procedure will be discussed in Chapter 5.

4.5.1 Results and Discussion

The design given in section 4.5 is considered. FEKO was used to calculate the scattering parameters. The scattering parameters are good indication for reflection and transmission. i.e. energy losses. Figure 4.8 shows the reflection coefficients for the beam ports as the excitation is applied. Due to the symmetric geometry the scattering parameters will be calculated only for the ports 1- 4.

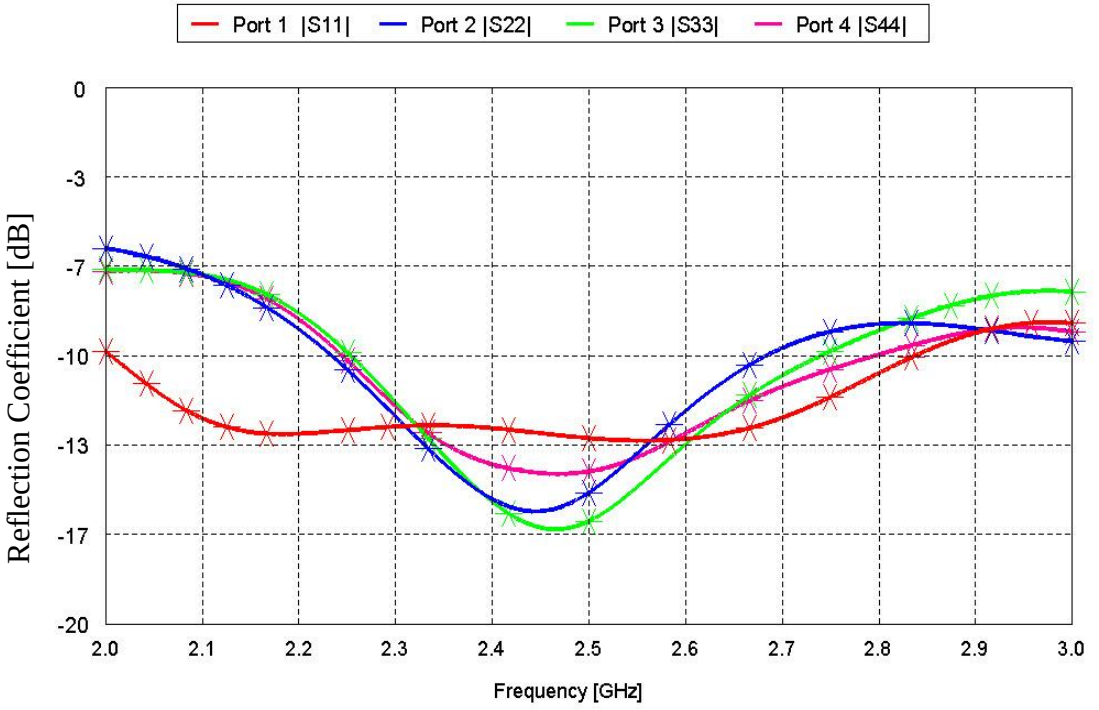

Figure 4.8: Reflection coefficients of the beam ports simulated by FEKO

Figure 4.8 shows that there is an acceptable return loss with design frequency 2.45 GHz for all input ports.

The next figures show the simulated transmission coefficients between the beam ports and the array ports simulated by FEKO. It is important to note that when a certain port is excited all the other ports are terminated with a matched load.

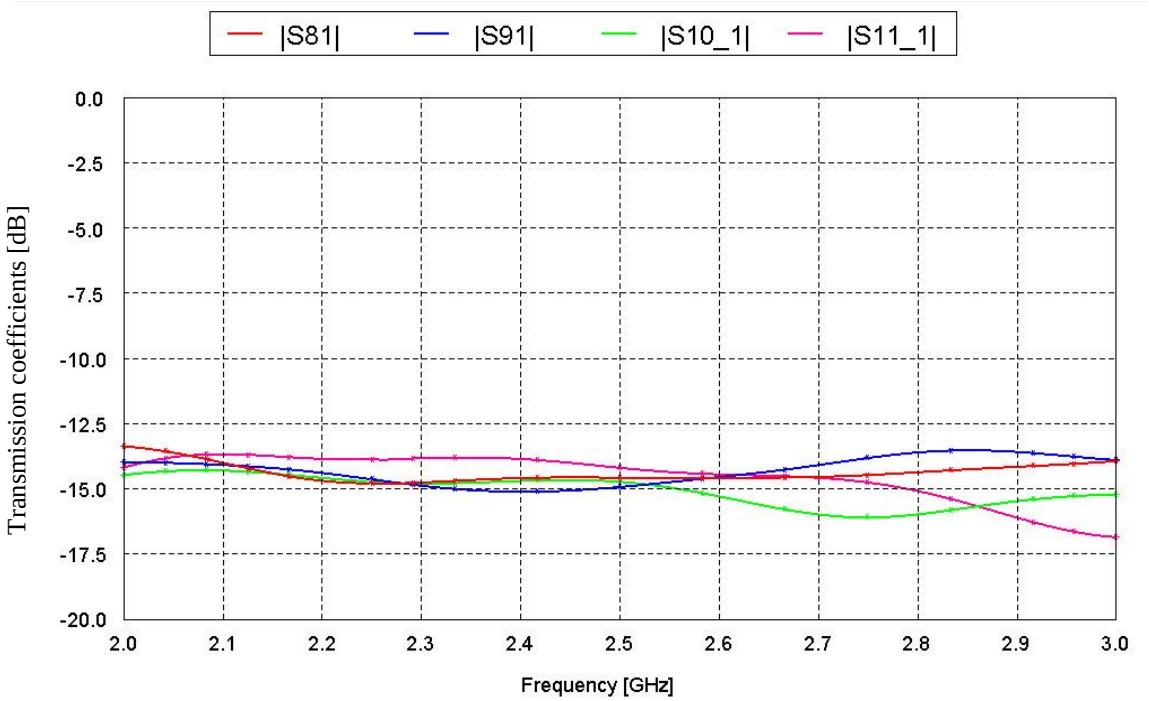

Figure 4.9: Transmission coefficients for port 1 excitation

A little energy fluctuations about 3dB can be realized from the results in Figure 4.8 and 4.9 between input port 1 and port 2 and the array ports.

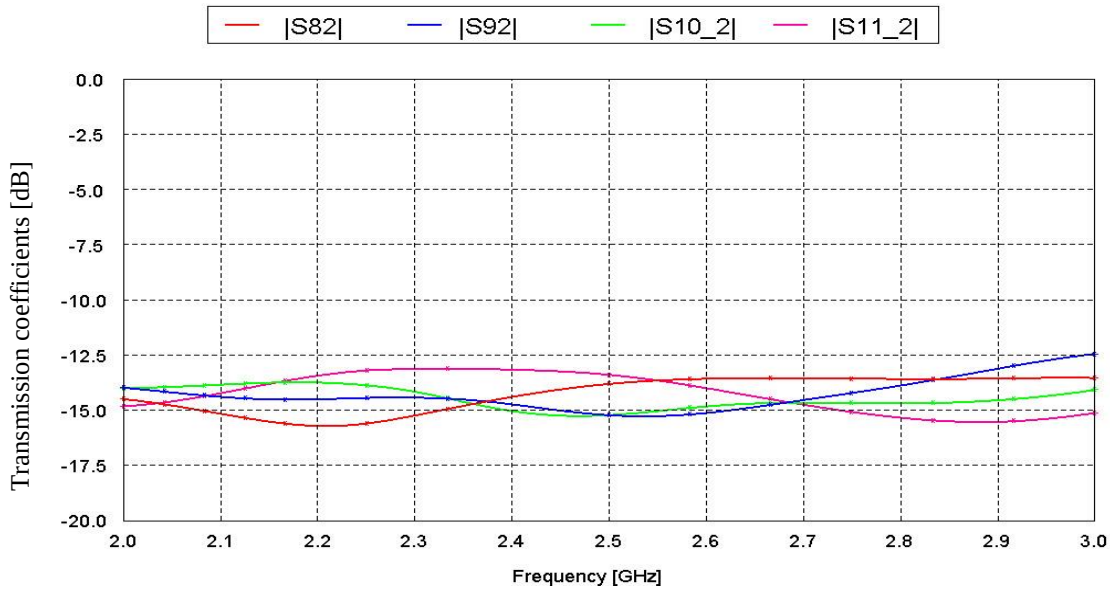

Figure 4.10: Transmission coefficients for port 2 excitation

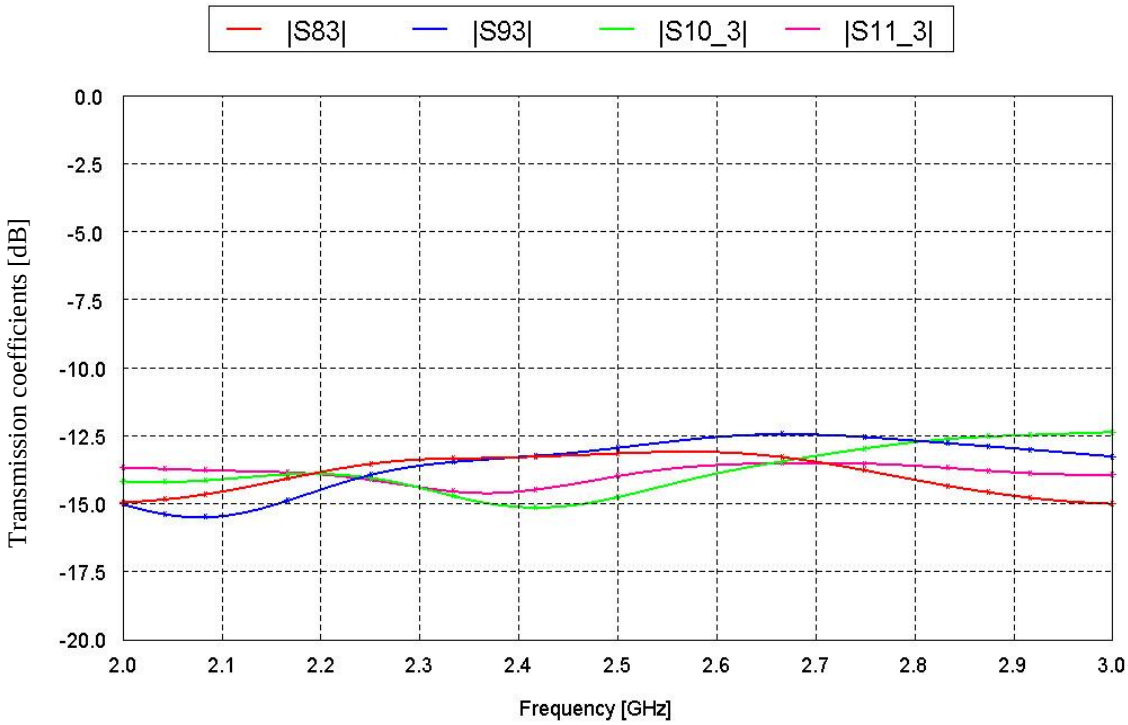

Figure 4.11: Transmission coefficients for port 3 excitation

Also when port 3 and port 4 was excited, small energy fluctuations between input ports and the receiver ports can be realized as shown in Figure 4.10 and Figure 4.11.

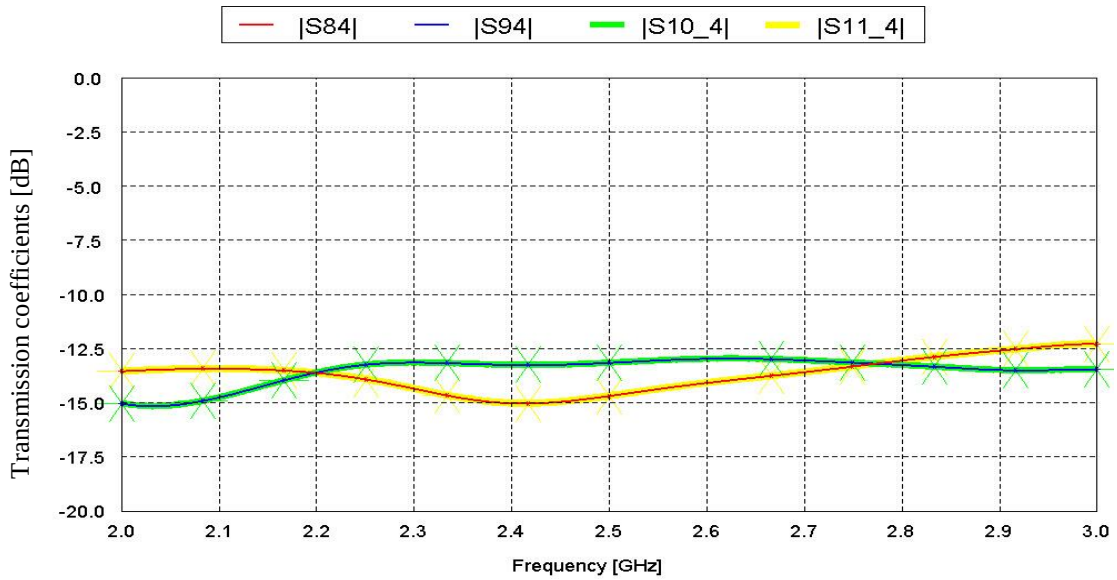

Figure 4.12: Transmission coefficients for port 4 excitation

Port 4 has identical transmission coefficient response with symmetrical array ports as shown in Figure 4.11.

The uniform amplitude energy is an important parameter in the lens design to achieve reasonable and uniform steering beam pattern. Figures (4.9)-(4.12) show that the amplitude of the transmission coefficients is almost uniform, indicating that most of the energy reach the beam ports. For the band from 2-3 GHz a small error, approximately 3dB error is observed.

The second important parameter is the phase simulation results of the lens. The optimum phase desirable for lens design is to achieve a linear shift with less error to obtain a uniform steerable radiation pattern.

The lens design equations are based on the geometric optics. Each beam ports produce a unique phase specification that directs the radiation pattern to a certain direction to attain the coverage of the desired area. Many studies have been carried out to optimize the design equation and reduce the phase error [20] [30] , as this study is not concentrate on this topic.

The next figures will explain the phase simulation results between the beam ports and the array ports.

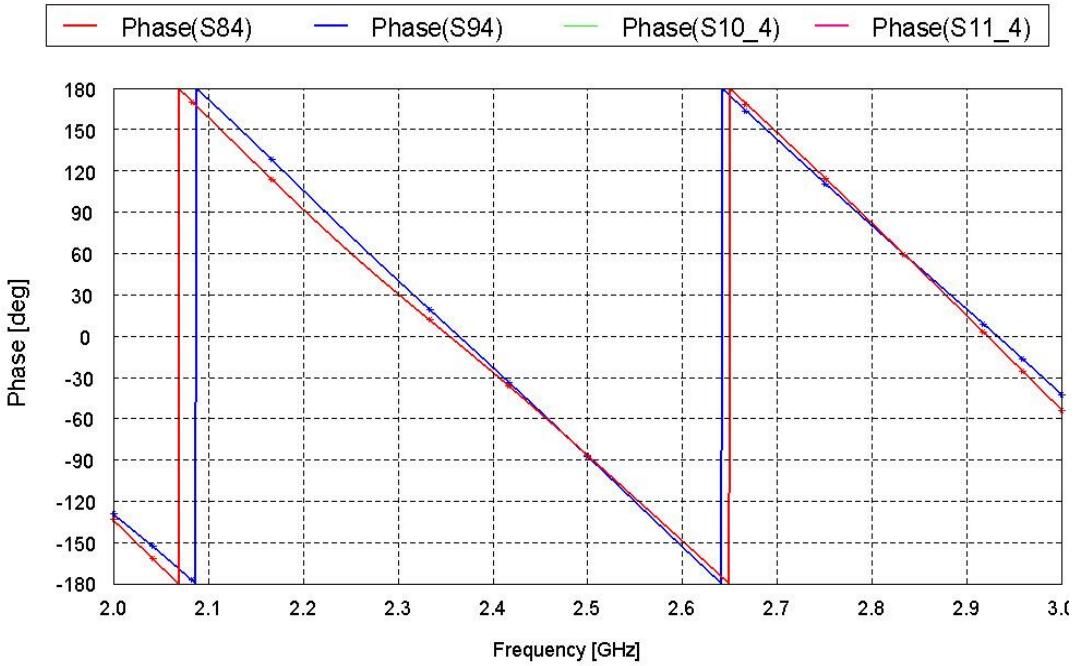

Figure 4.13: Port 4 phase simulation result by FEKO

Figure 4.13 describes the phase simulation when the center port (port 4) was excited. Due to the symmetrical geometry of the lens only the output phase of the ports 8 and 9 are shown. According to the geometric optics of the lens design equations, when the center port of the lens was excited the phase reached to the array ports will be the same, so the result shows this agreement at the design frequency 2.45GHz, the array ports are in phase when the center port was excited.

The radiation pattern of the array elements will be symmetrical according to the array center position when center port was excited. In other words, the angle of the steering radiation pattern will be equal to the zero as will be explained in the next sections.

As it is mentioned before, every beam port is designed to produce a pattern in a certain direction. Figure 4.14 explains the phase simulation result when the beam port 1 was excited.

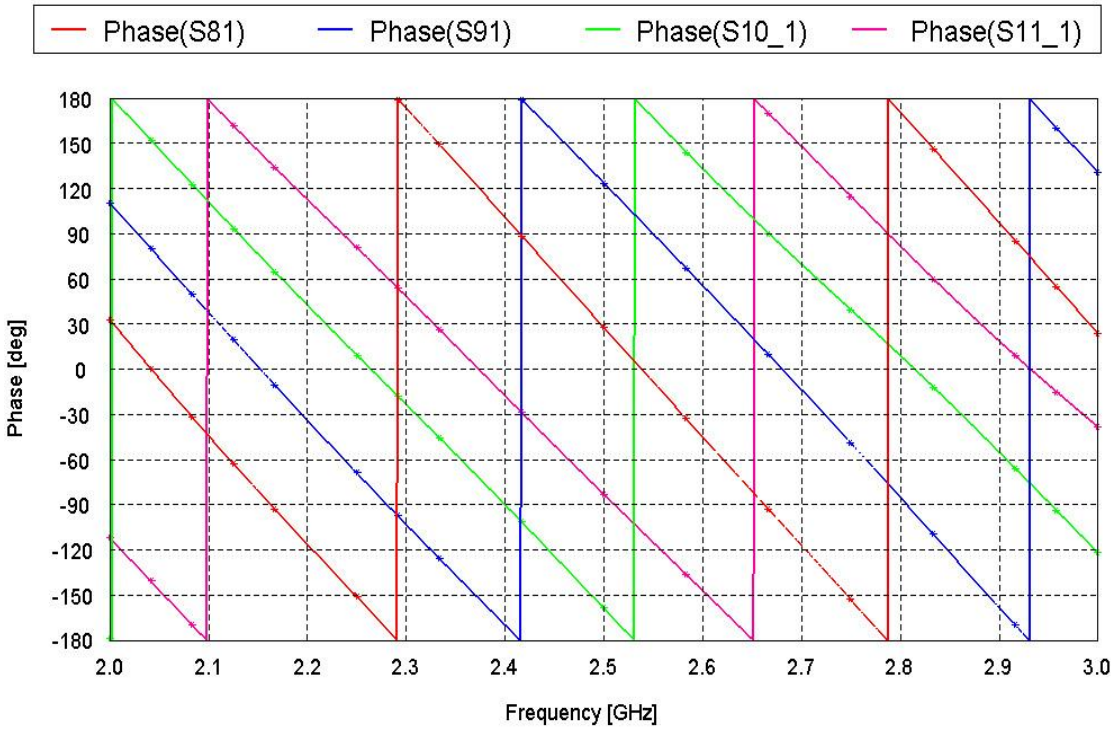

Figure 4.14: Port 1 phase simulation result by FEKO

The surface current distribution of the lens can further explain the phase and current amplitude of the lens. The distribution of the current amplitude and phase when the switching was applied between the beam ports are illustrated in Figure 4.15 and 4.16.

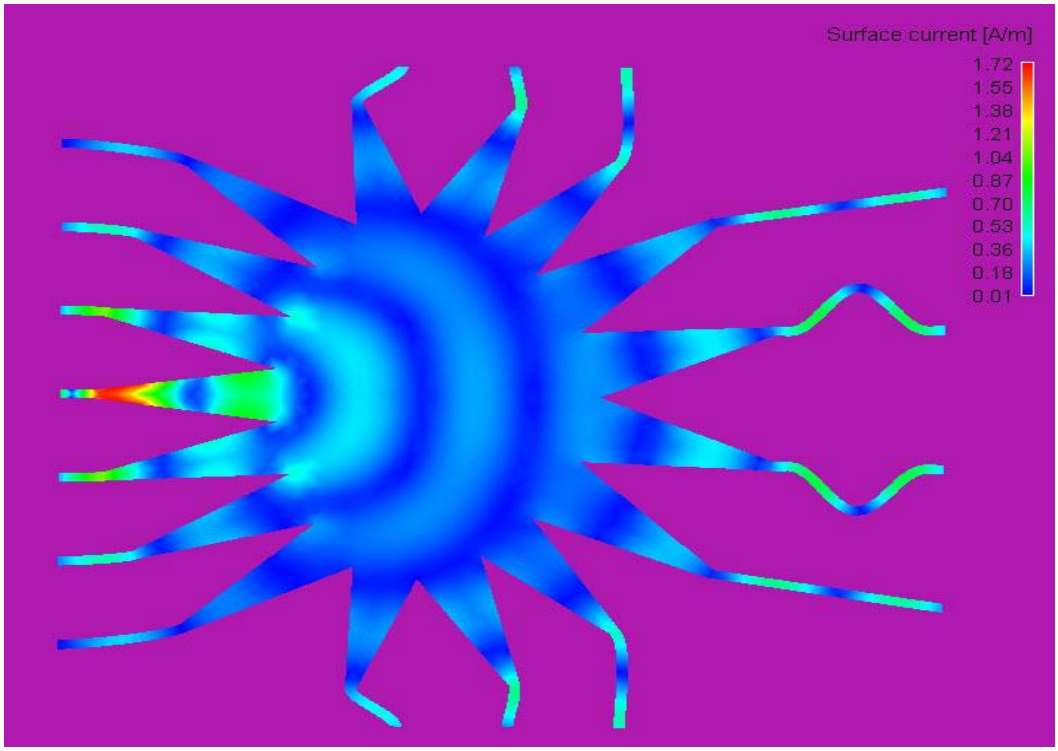

Figure 4.15: Surface current for port 4 excited with 2.45GHz simulated by FEKO

The surface current when switching was applied between ports 4 and 1 is explained in Figure 4.15 and Figure 4.16.

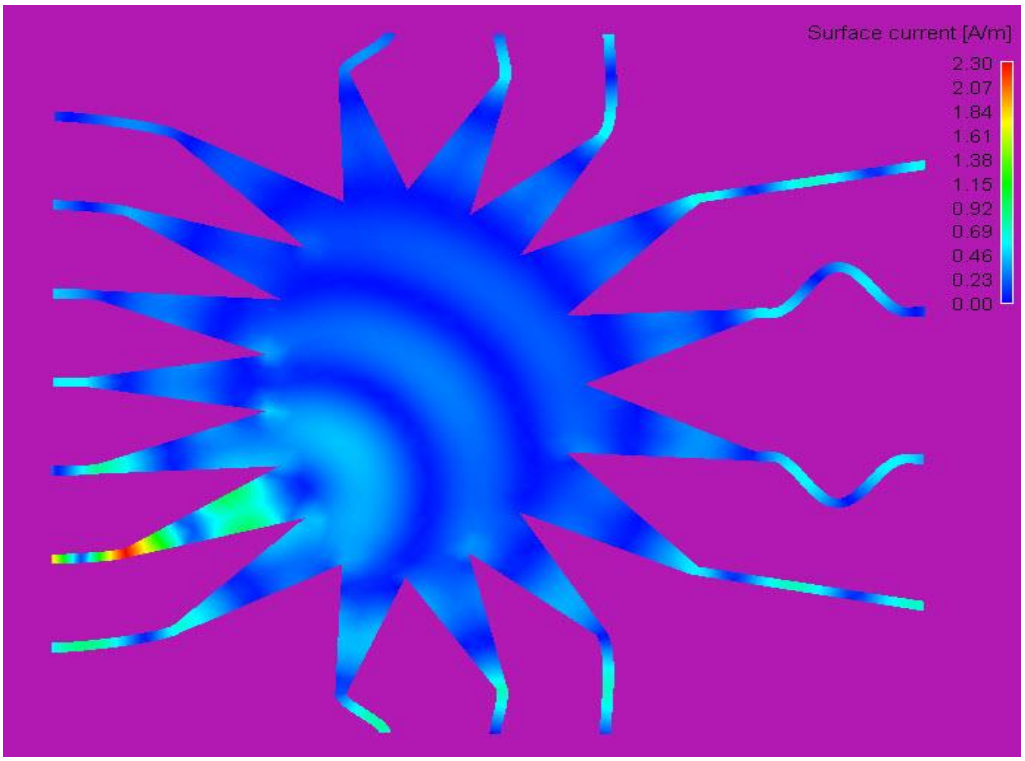

Figure 4.16: Surface current for port 2 excited with 2.45GHz simulated by FEKO

The dummy ports and the side walls are designed to absorb the fields and reduce the incident reflection within the lens [28]. The number of the dummy ports and the shape of the side wall are considered as design parameter. However, these dummy ports can be replaced with an absorbing material. Figure 4.17 shows an example of a poor side wall design model; reflected waves from the edge of the side walls appear clearly when port 1 was excited.

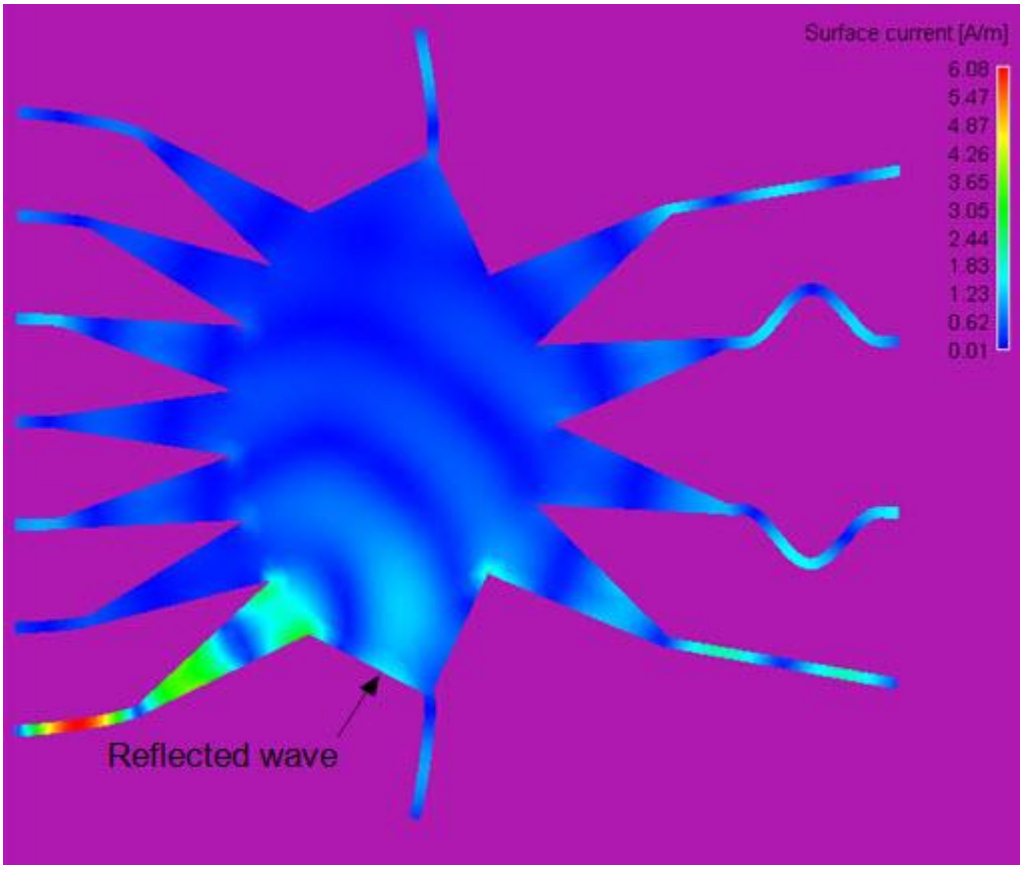

Figure 4.17: Incident reflected wave for improper side wall design

The beam forming system as it is explained is used to obtain radiation in required directions. To illustrate the multiple beams forming, a bowtie antenna will be designed and connected to the lens.

4.5.2 The Bowtie Antenna Design

In this section bowtie antenna will be designed to work as a radiator element for the lens. The specifications of the design are shown in the table below.

Table 4.4: Bowtie design parameters

Center frequency	Relative permittivity (FR4)	Substrate thickness	Loss tangent
2.45GHz	4.4	1.6	0.02

The formula for designing bowtie antenna can be derived by considering the microstrip and the substrate as a wave guide [31]. The design formula is given by Equation (4.12).

$$f_{m,n} = \frac{2 \times c}{3 \times a \sqrt{\varepsilon_r}} \sqrt{m^2 + m\ n + n^2} \qquad (4.12)$$

Where: f is the center frequency, m=1 and n=1 for microstrip, ε_r : is the relative permittivity, c: light speed= 3×10^8 m/s and a: is the side length of the bowtie.

The above formula is used to determine the initial antenna dimensions of the bowtie and theoretical calculation still needed more optimization to get accurate result. Figure 4.18 shows the final bowtie geometry and its dimensions.

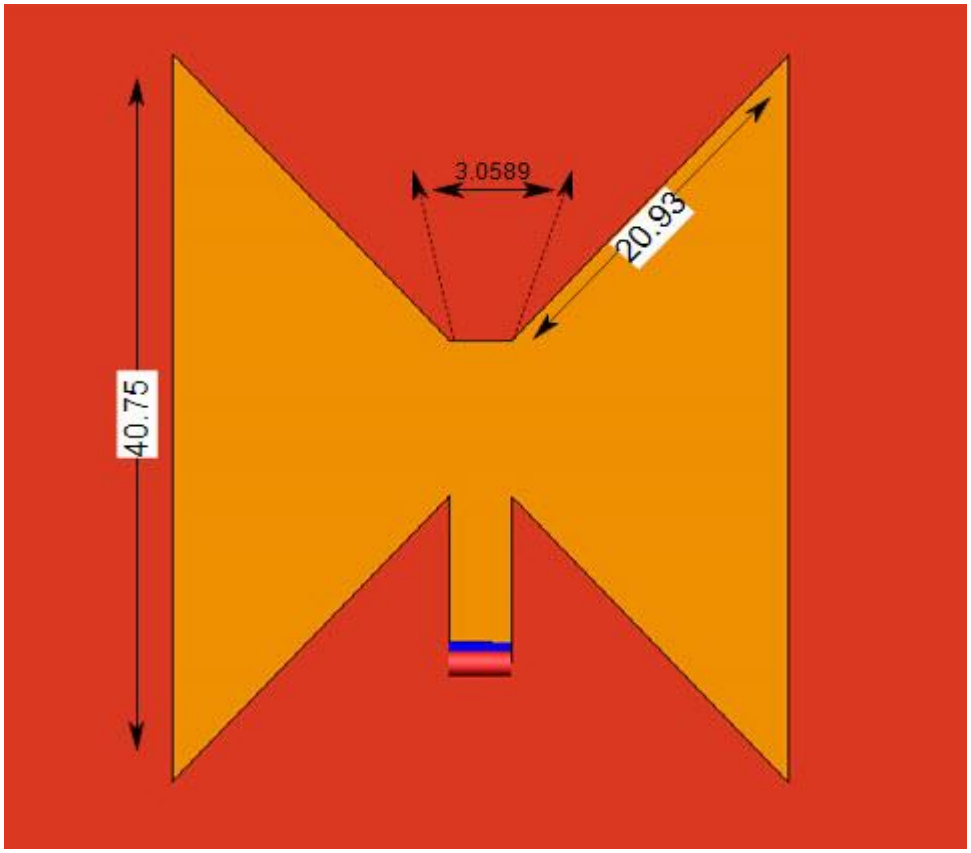

Figure 4.18: Bowtie antenna FEKO model dimensions in mm

The reflection coefficient at the input terminal is shown in Figure 4.19. The return loss of 2.45 GHz is 30dB.

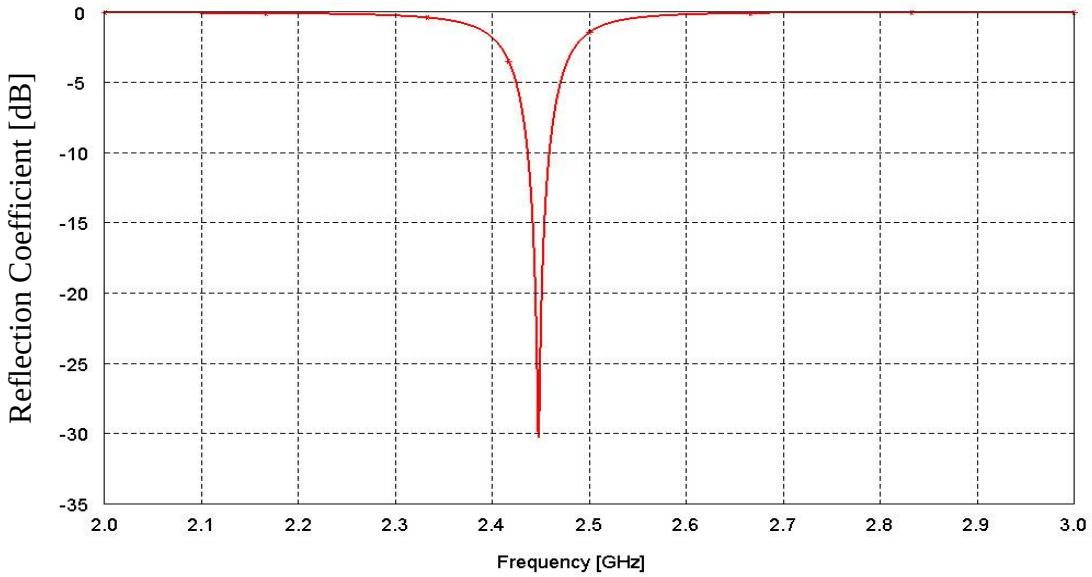

Figure 4.19: Input reflection coefficient of the Bowtie antenna

The radiation pattern and gain are shown in Figure 4.19 and Figure 4.20 with gain approximately 6dB.

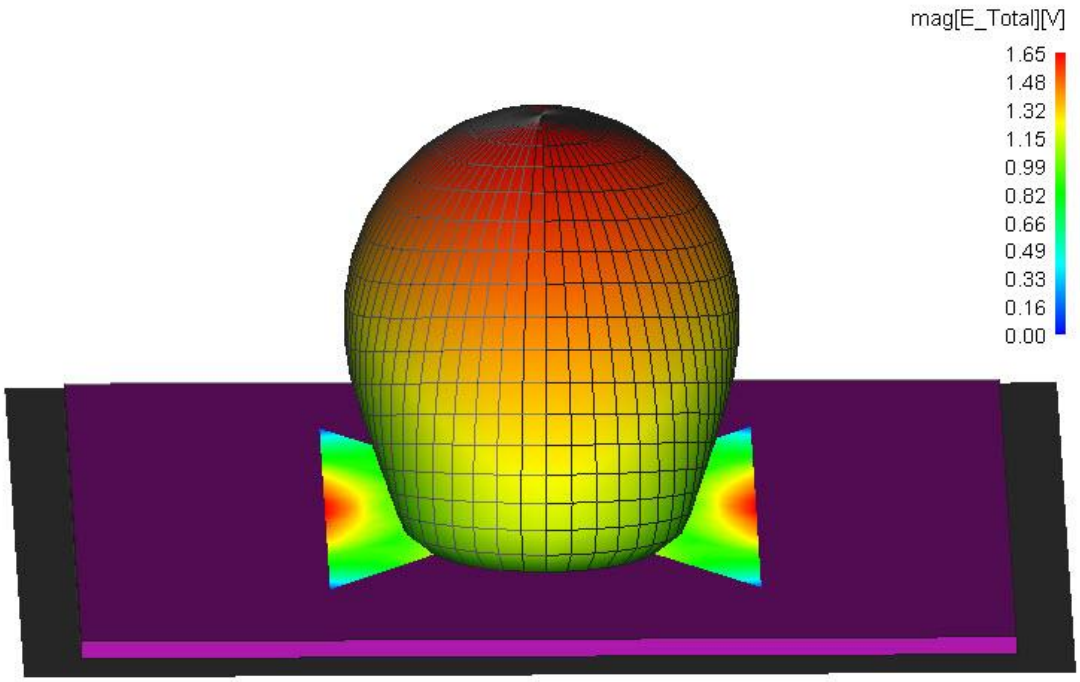

Figure 4.21:3-D Radiation pattern of Bowtie antenna

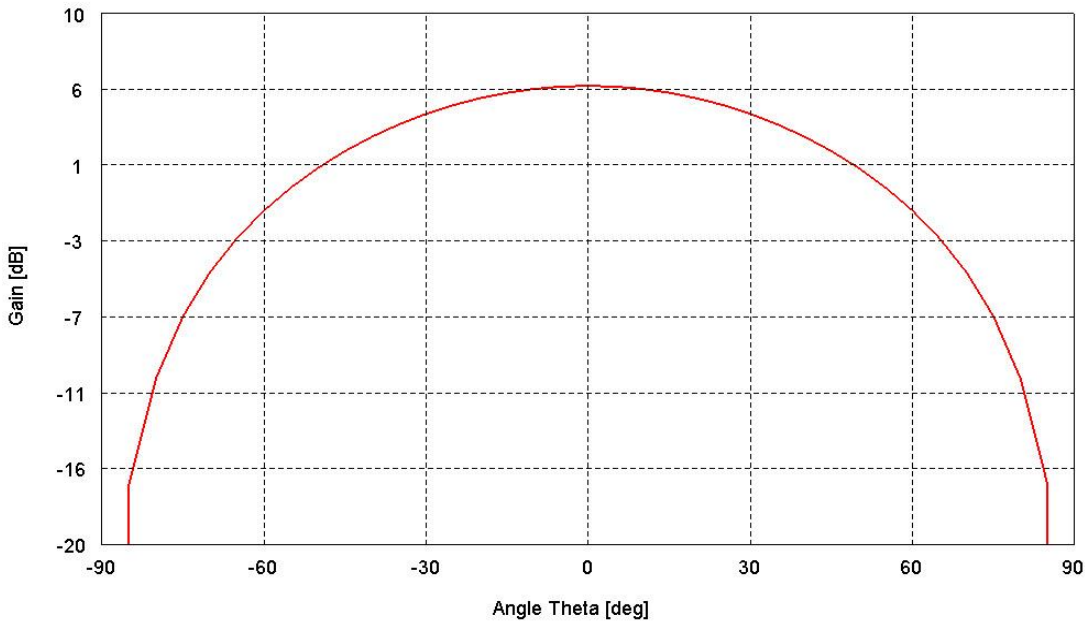

Figure 4.20: Bowtie antenna gain

4.5.3 Lens with Bowtie Antenna

The beam forming system described in Chapter 2 is a multiport device used for controlling the beam direction of the phased array antenna by switching the excitation on the input ports; to illustrate the system, the lens connected with radiator antenna elements is shown in Figure 4.22.

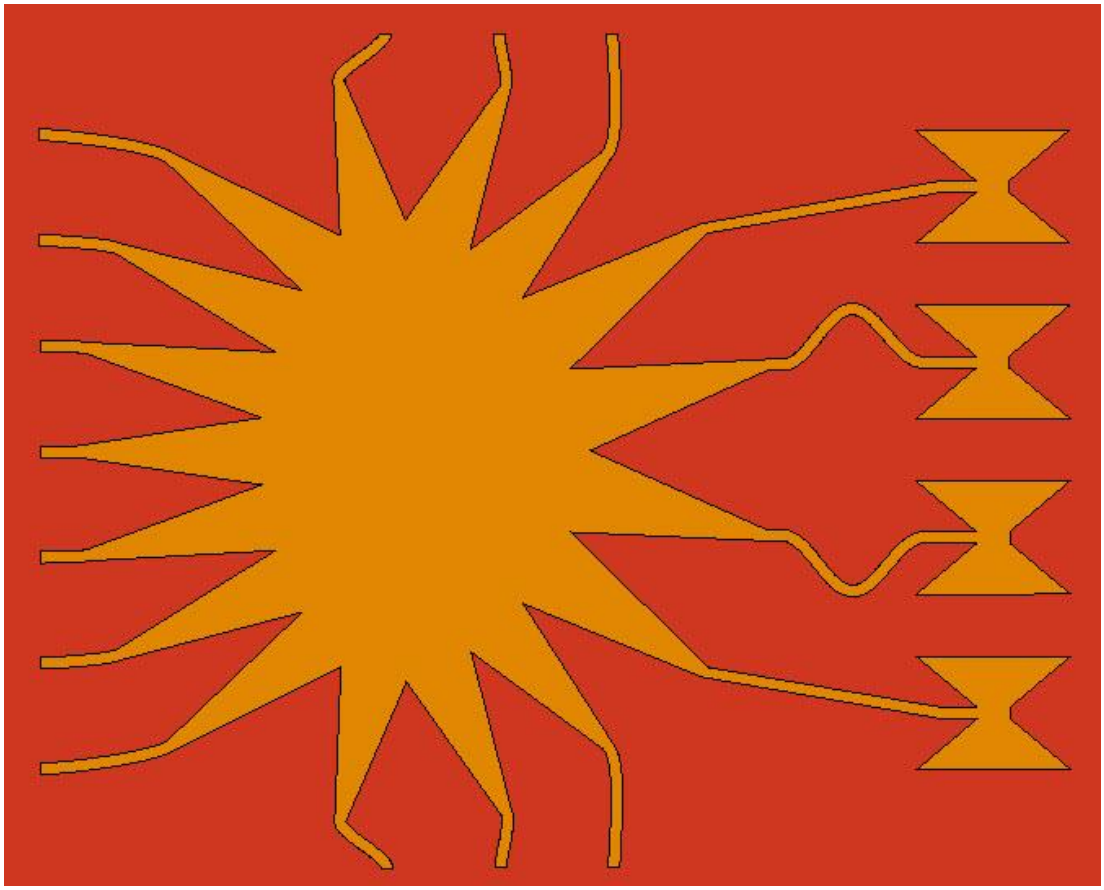

Figure 4.22: Lens connected with radiator antenna

After connecting the antenna elements to the lens, optimization process has been carried out for tapering the microstrip line to decrease its length with acceptable return loss. Matching method and the tapering design procedure will be discussed in Chapter 5. The modified lens is shown in Figure 4.23.

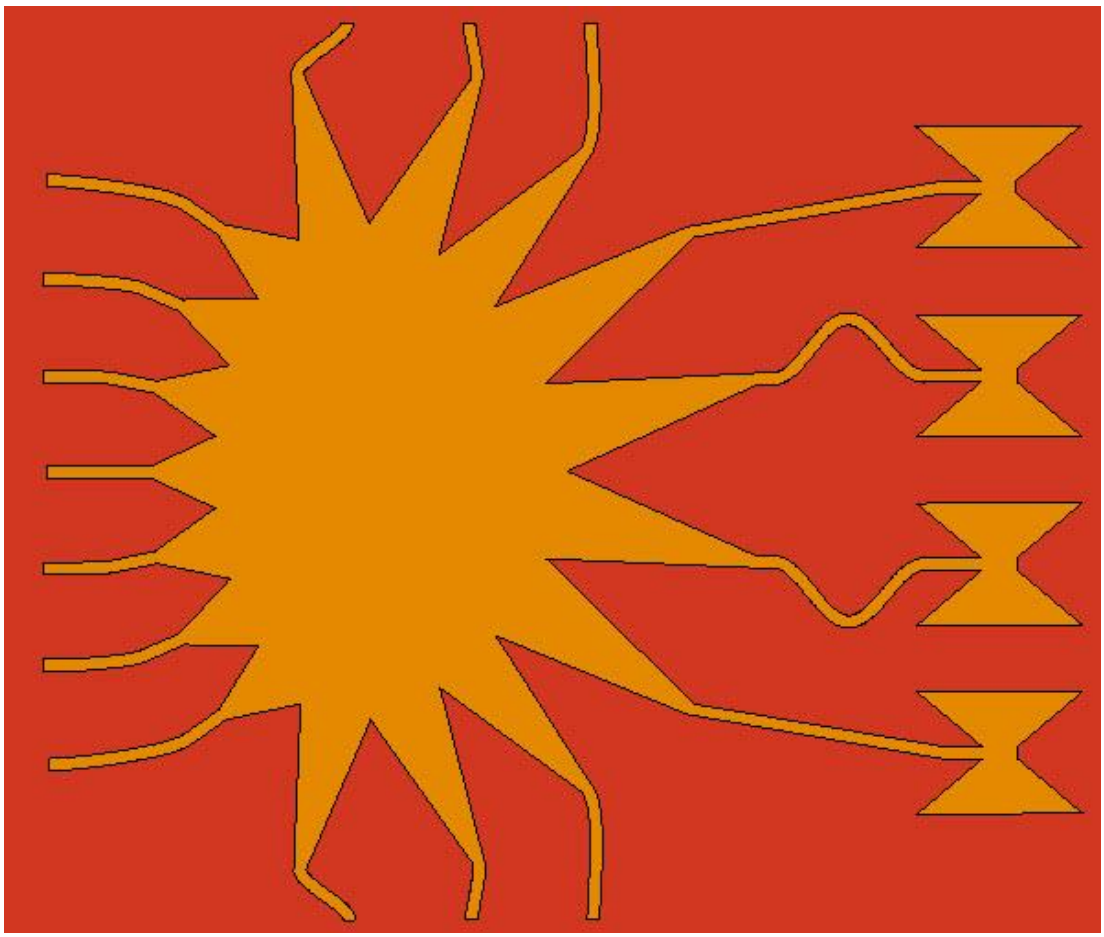

Figure 4.23: Modified tapered beam ports of the lens with bowtie antenna

The excitation was applied to each beam port separately. During the simulation, all of the ports which were not connected to the voltage source were connected to 50Ω load to decrease reflections.

Figures 4.24, 4.25 and 4.26 explain the change in the beam direction when the switching process was applied to the beam ports at 2.45 GHz.

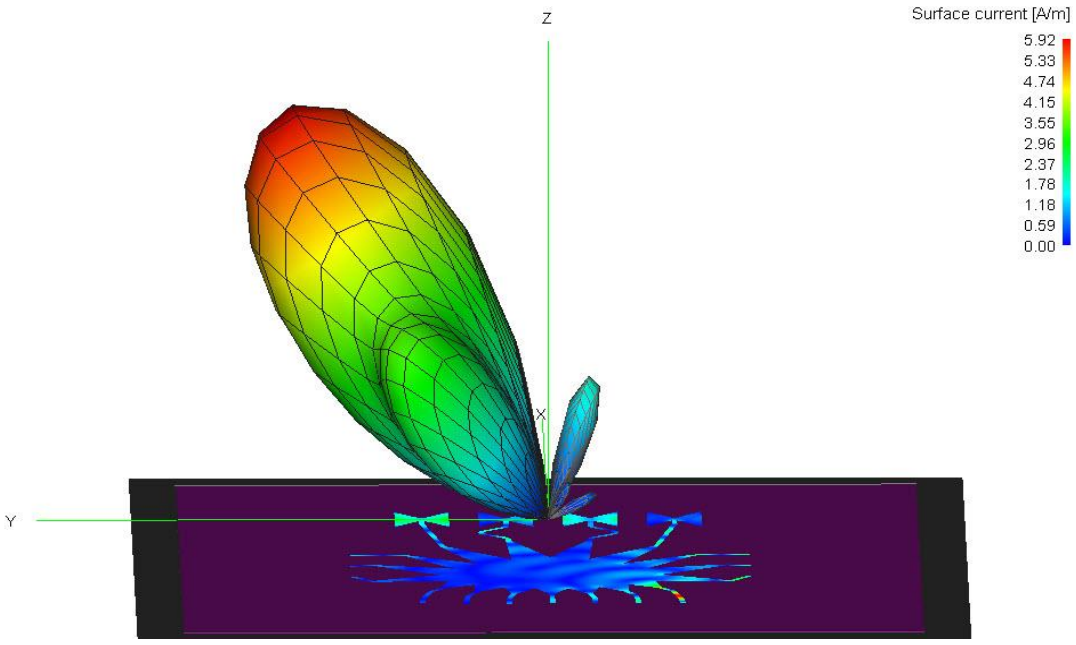

Figure 4.24: Surface current and 3-D radiation pattern for port 1 excitation

The beam direction is normal to the array elements when the center port (port 4) was excited. Figure 4.25 demonstrates the radiation pattern normal to the antenna elements as well as the surface current on the lens surface.

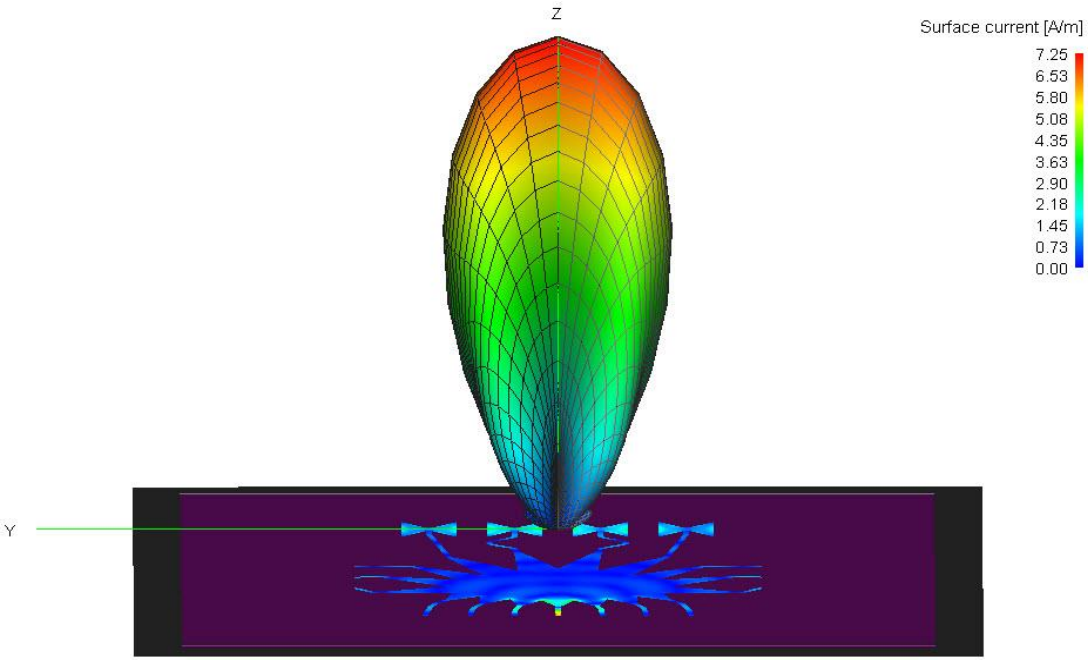

Figure 4.25: Surface current and 3-D radiation pattern for port 4 excitation

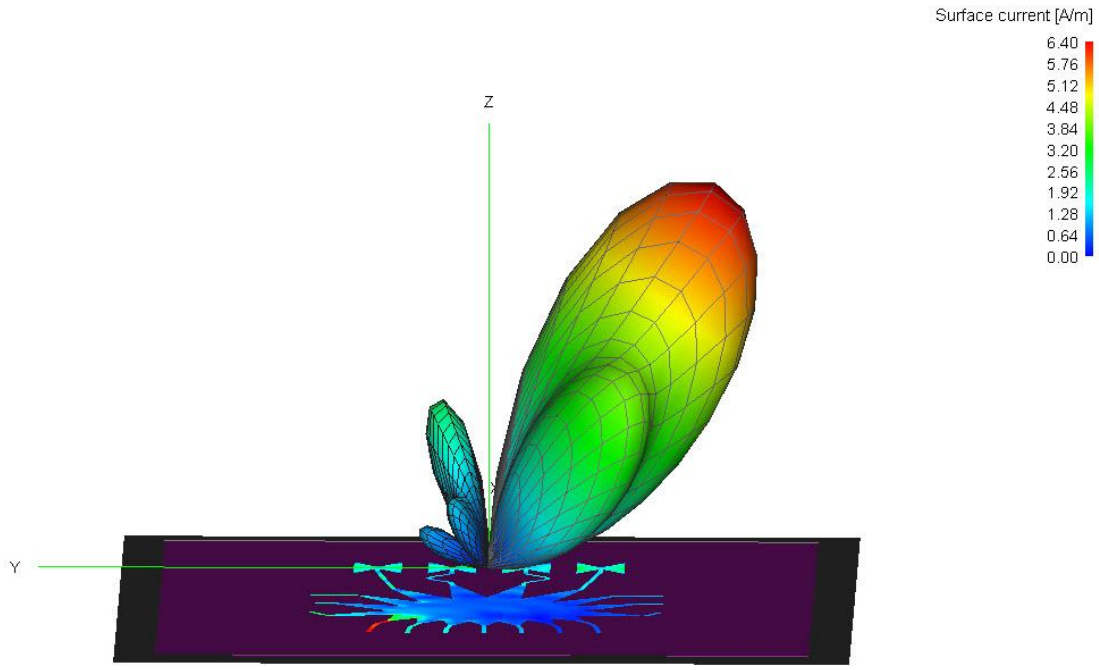

Figure 4.26: Surface current and 3-D radiation for port 7 excitation

The beams shown in Figure 4.27 and Figure 4.28 belong to the input ports. Figure 4.27 shows the cartesian plot while in Figure 3.28 polar plot technique have been used.

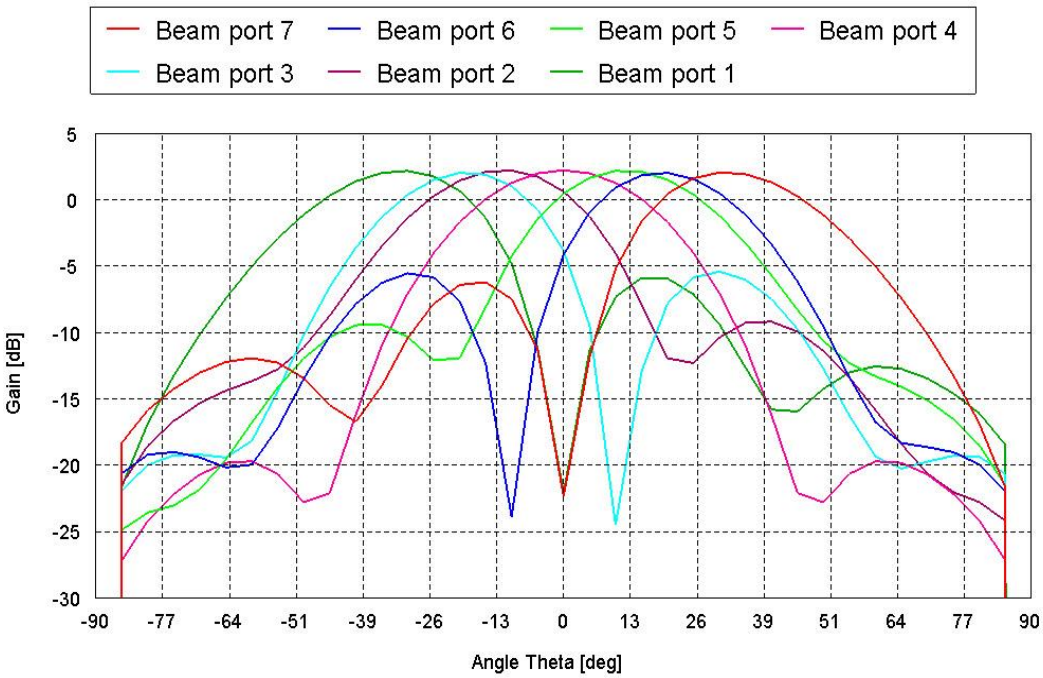

Figure 4.27: The multiple gain beams at 2.45GHz Cartesian plot

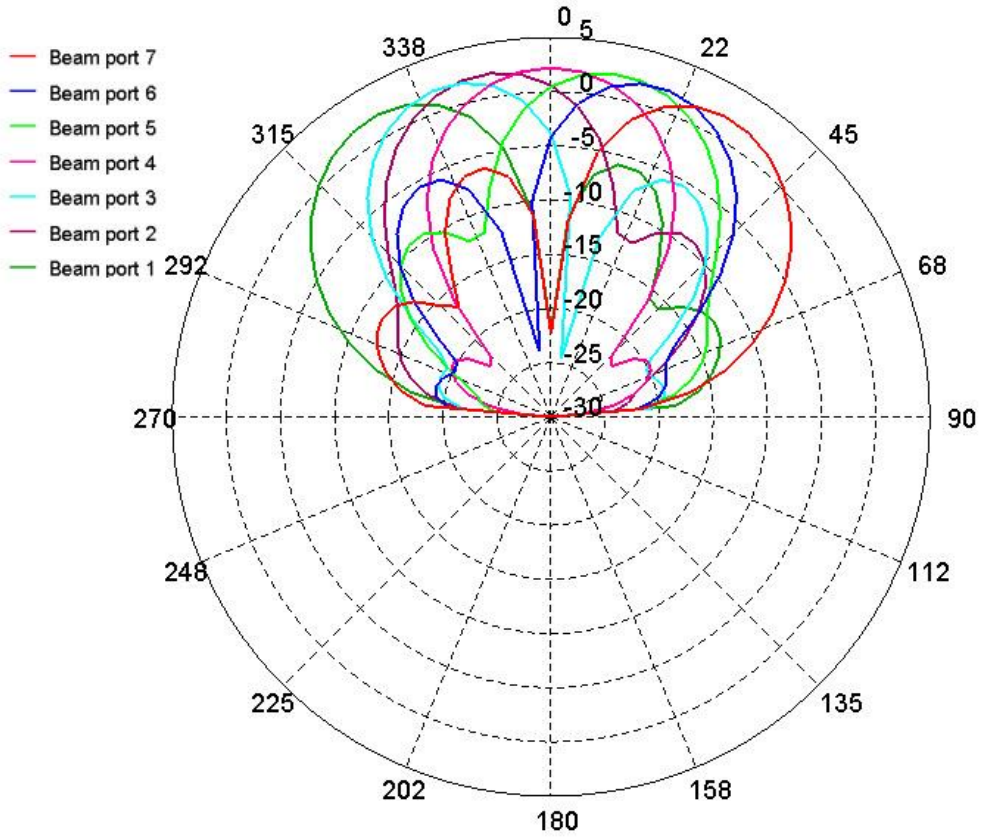

Figure 4.28: The multiple gain beams at 2.45GHz Polar plot

The simulated results explain the change in the beam direction according to the switching of the excitation between the input ports, to form the seven beams in different directions. The results show that, although fixed array antenna elements have been used, the required scan angle was achieved by producing different beams covered from 35° to -35° angle with a gain about 2.5dB.

Chapter 5

LENS MATCHING TECHNIQUES

5.1 Matching Overview

In the microwave circuit the matching between the source and the load is very important because imperfect matching increases reflection. The phase performance and the power losses are also important factors related with mismatching.

This chapter covers the techniques used to match the lens geometry impedance with 50Ω impedance of the transmission line. The general matching circuit diagram is shown in Figure 5.1 [3].

Figure 5.1: Matching circuit diagram

The lens has lower impedance compared to the transmission line because it's surface is wider surface than the transmission line. The procedure of matching is to attain a gradual energy transformation between the transmission lines and the lens to reduce the return loss. In following, the taper models and the procedure implementation designs will be explained.

5.2 Horn Taper Model Implementations

5.2.1 Linear Tapering Model

This tapering model is considered as the simplest and popular model that is used with lens geometry. The design equation is shown below by Equation (5.1).

$$Z(z) = Z_0 z + s \qquad 0 < z < L,\ s \neq 0 \tag{5.1}$$

The relationship between the design parameters, characteristic impedance Z_0, the load impedance Z_L and the taper length L are shown in Figure 5.2.

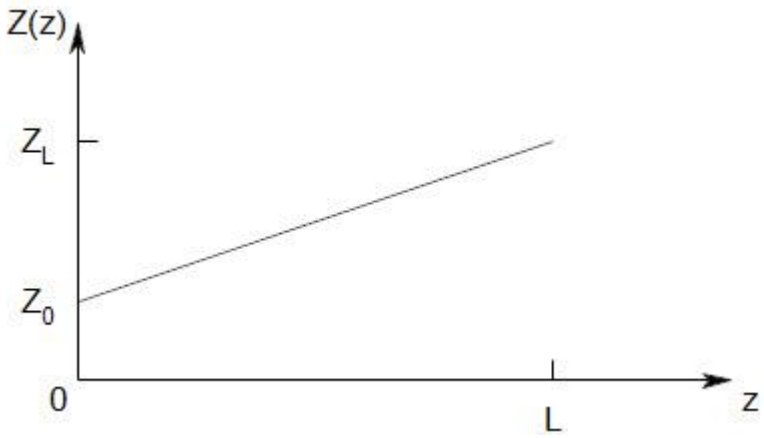

Figure 5.2: The relations between the linear taper design parameters

.

The geometry of the linear taper designed by FEKO is shown in Figure 5.3.

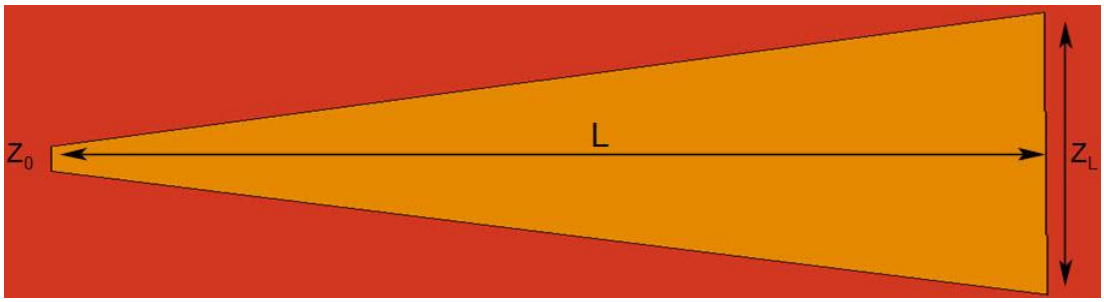

Figure 5.3: Linear taper (FEKO model)

5.2.2 Exponential Model

The geometry of the exponential taper is shown in Figure 5.4. A smooth energy transition between the source and the load can be achieved by using this model.

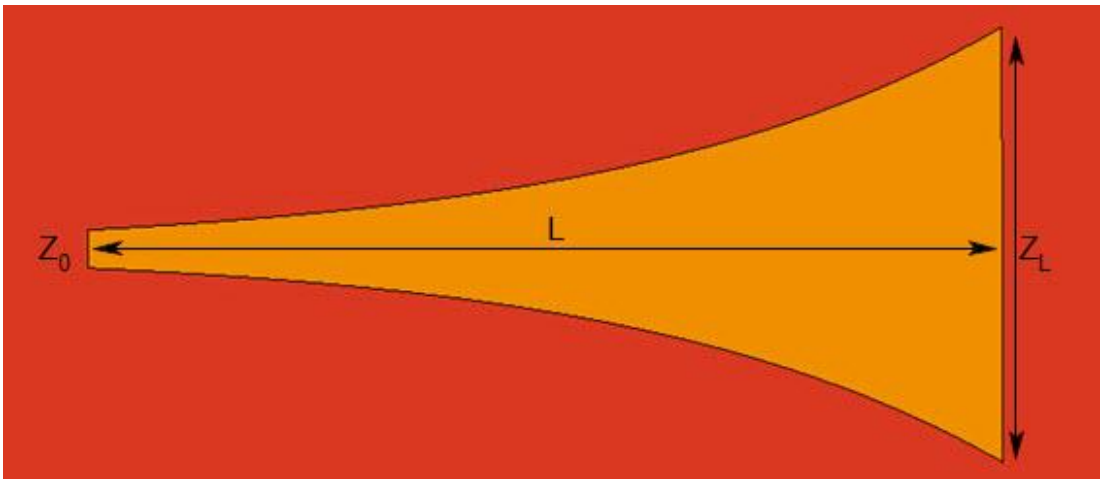

Figure 5.4: Exponential taper (FEKO model)

The relationship between the design parameters, the characteristic impedance Z_0, the load impedance Z_L and the taper length L are shown in Figure 5.5 [3].

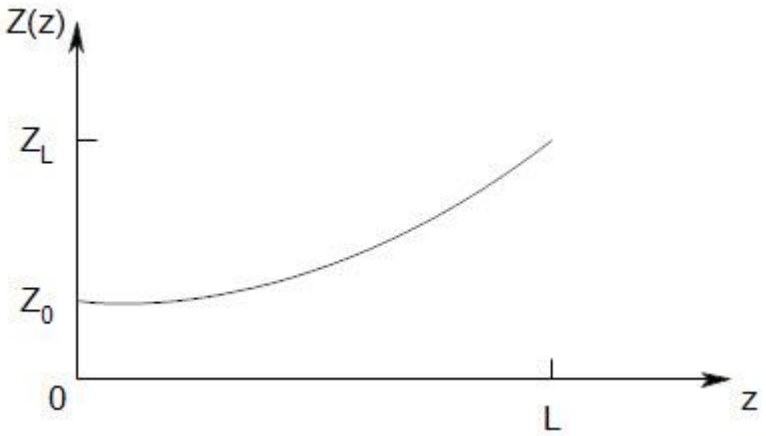

Figure 5.5: The relations between the exponential taper design parameters

The design equations of the exponential taper are shown below:

$$Z(z) = Z_0 e^{a z} \qquad 0 < z < L \tag{5.2}$$

$$a = \frac{1}{L} \ln\left(\frac{Z_L}{Z_0}\right) \tag{5.3}$$

5.2.3 Triangular Model

The design equation of this type is more complicated compared to the exponential model; the taper length is divided in two parts, each part has its equation design as described by Equation (5.4).

$$Z(z) = \begin{cases} Z_0 e^{2(z/L)^2 \ln Z_L/Z_0} & 0 \le z \le L/2 \\ Z_0 e^{(4z/L - 2z^2/L^2 - 1)\ln Z_L/Z_0} & L/2 \le z \le L \end{cases} \tag{5.4}$$

The relationship between the design parameters, characteristic impedance Z_0, the load impedance Z_L and the taper length L are shown in Figure 5.6.

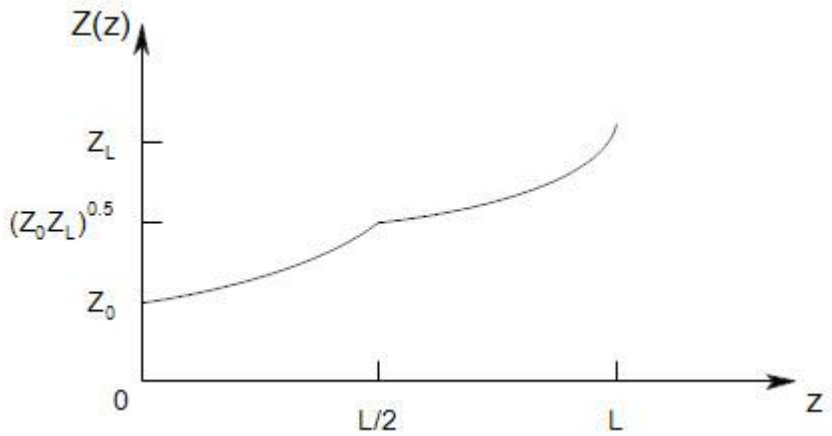

Figure 5.6: The relations between the triangular taper design parameters

The geometry of the triangular taper designed by FEKO is shown in Figure 5.7.

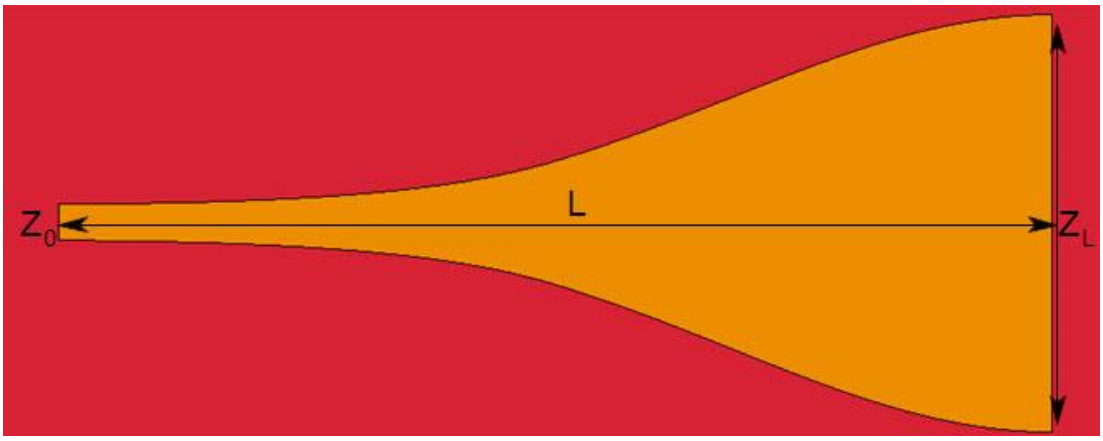

Figure 5.7: Triangular taper (FEKO model)

5.3 Simulation Results

The return loss of the linear, exponential and triangular taper types will be examined for matching between the given characteristic impedance Z_0 and the load impedance Z_L. In this simulations bandwidth (1 GHz -6 GHz) is considered as suggested by Dong [2].

The taper parameters including substrate properties, side widths and taper length are given by Table 5.1.

Table 5.1: Taper specification design [2]

Substrate permittivity	Substrate thickness	W_0	W_L	Taper length
2.33	0.508mm	1.82mm	20.8mm	49.5mm

Where: W_0 is the width of the transmission line from source side and W_L is the width of the transmission line from load side. Figures (5.8-5.10) show FEKO taper geometry models.

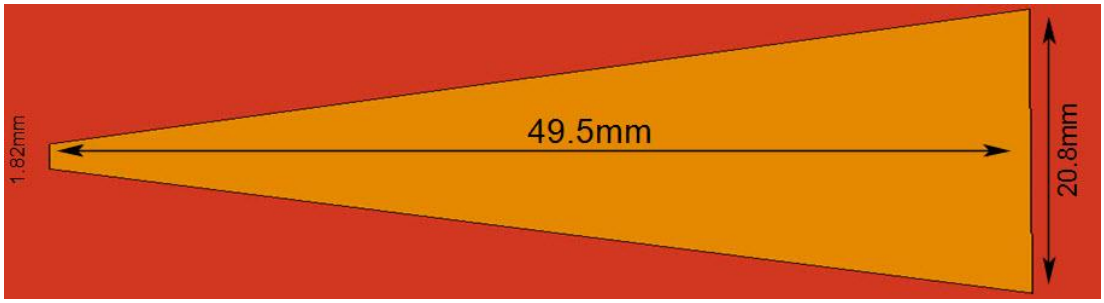

Figure 5.8: linear model

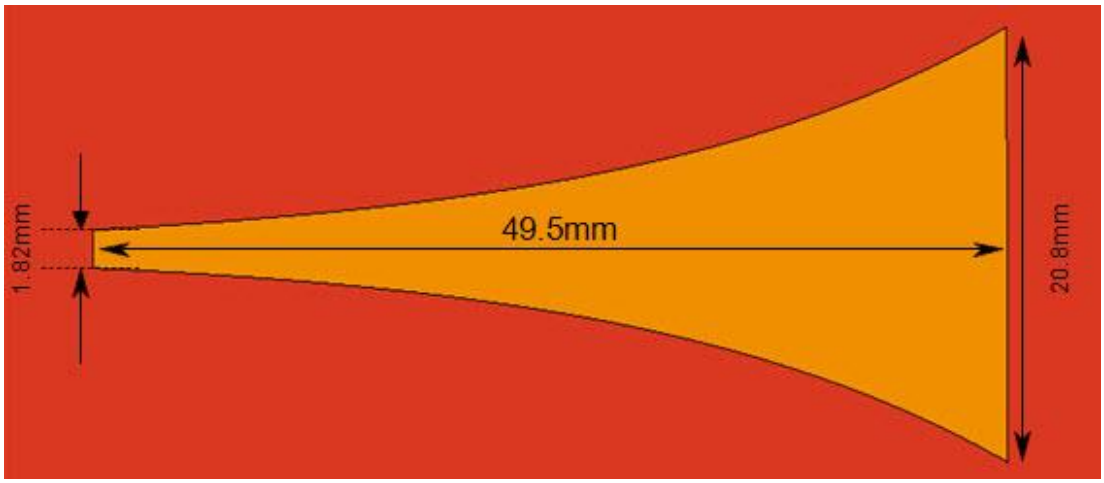

Figure 5.9: Exponential model

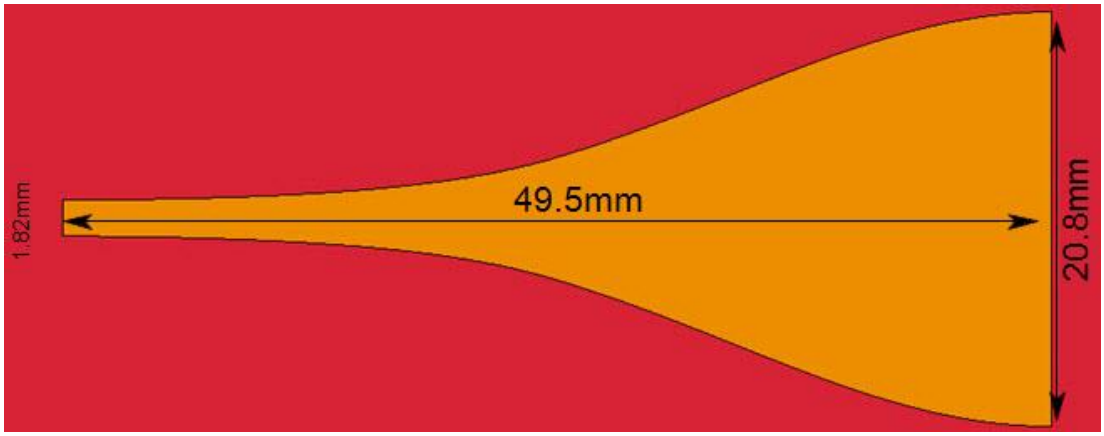

Figure 5.10: Triangular model

The reference paper result of the linear taper simulation is shown in Figure 5.11. The FEKO simulated results for all three types are shown in Figure 5.12.

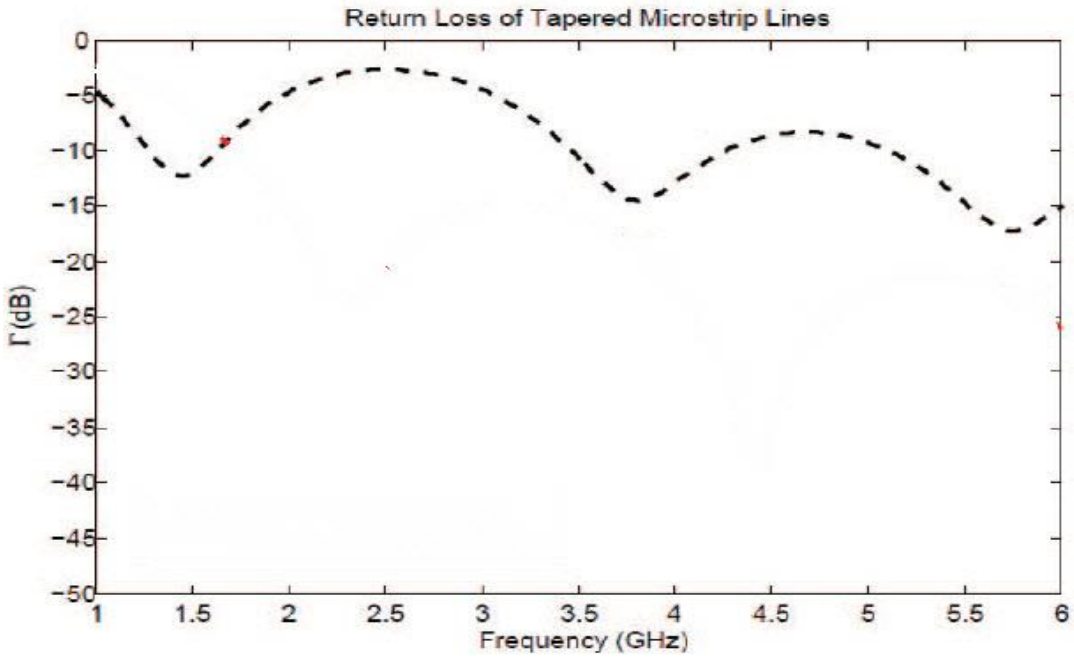

Figure 5.11: Linear taper reflection coefficient [2]

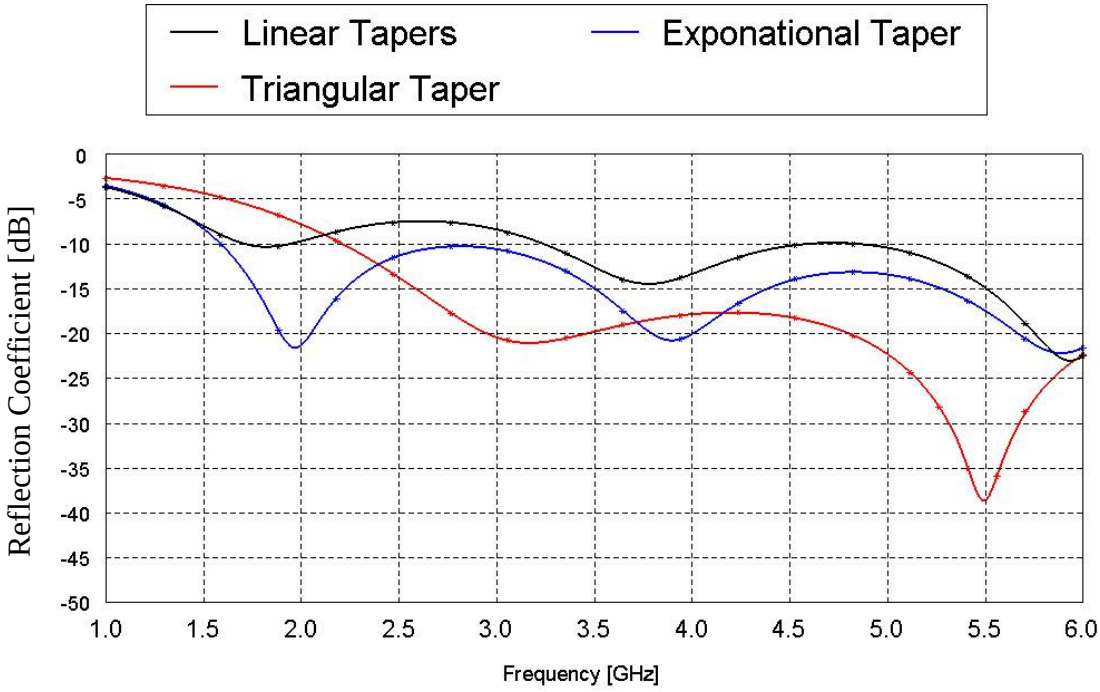

Figure 5.12: Reflection coefficients of three tapering models simulated by FEKO

There is an agreement between the two results of the linear taper return loss for given by Dong and results simulated by FEKO given by Figure 5.11 and Figure 5.12. However, the results of linear, exponential and triangular tapers describe that each

taper type has different return loss response for the equal dimensions and design parameters specification (i.e. substrate thickness and relative permittivity).

In practice, tapering is used for matching between 50Ω characteristic impedance and specific load impedance. The two side widths of the taper are considered as given parameters and the characteristic impedance calculated by Equations (4.10) and (4.11) which are explained in Chapter 4.

The taper length is the main parameter that has an effect on the value of the reflection coefficient and it is considered as undetermined variable. The procedure to calculate the taper length is to use optimization method to achieve acceptable return loss with a certain length. Optimisation process needs a computer with high performance ability of the core process unit to save the computation time.

The next section covers different approach for matching, by building a multi sections taper between the source and the load.

This method depends on the calculations of the standing wave pattern within the substrate below the conductor. The multi-section transformation was simulated by Uyguroğlu and Öztoprak using FDTD [32]. The idea is used here for the first time to match 50Ω transmission line to the parallel plate geometry using FEKO and then the same procedure will be applied to the lens geometry.

5.4 Lens as a Parallel Plate

Microstrip lens can be considered as a parallel plate cavity with aperture connected between parallel plate cavity and the microstrip feeding line as illustrated in Figure 5.13. The parallel plate edges are terminated by loads to reduce the reflection from the edges i.e. simulating large parallel plate region. The goal for this study is to match the feeding line impedance to Z_0=50Ω characteristic impedance with the aperture width which has Z_A impedance. This is achieved by an additional section with impedance Z_B with a certain length, as shown by Figure 5.14.

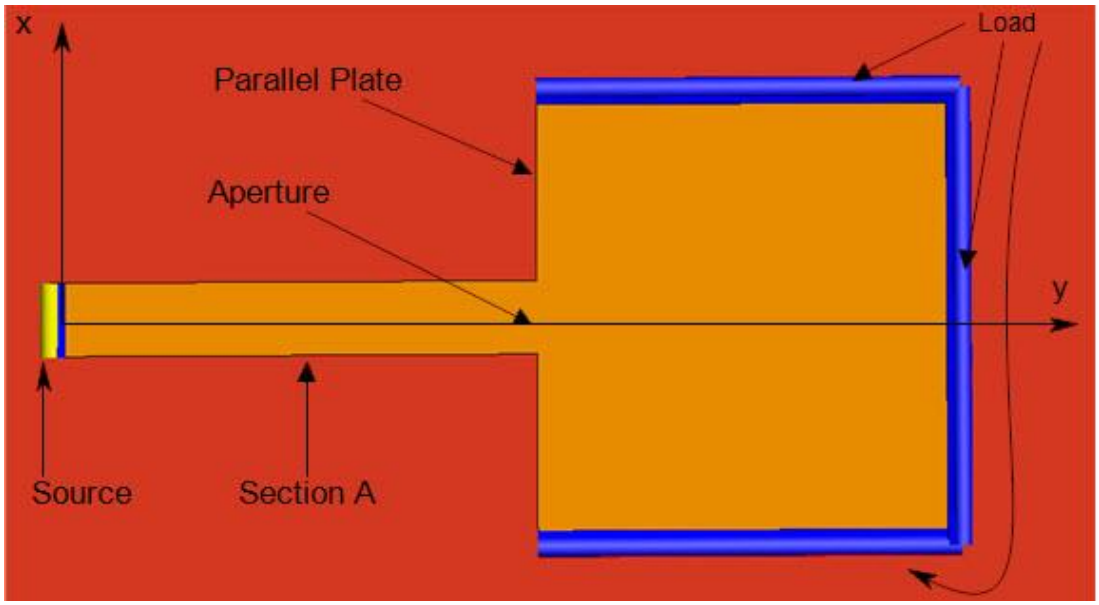

Figure 5.13: Parallel plate with microstrip feeding line

The design parameters and substrate specifications are listed in Table 5.2.

Table 5.2: Parallel plate design parameters

Frequency	Substrate permittivity	Substrate thickness	Aperture width	Parallel plate dimensions
5 GHz	4.4	1.6 mm	8 mm	50*50 mm^2

5.4.1 Taper Sections Implementations

The dimensions and impedances of the three sections transition are explained in Figure 5.14.

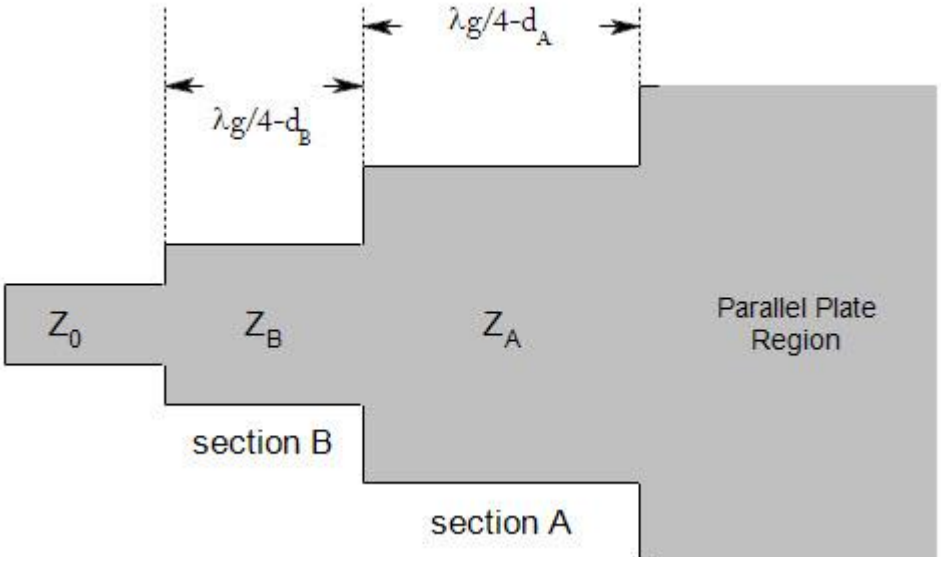

Figure 5.14: Transition between Z_0 and parallel plate region [32]

The matching between Z_0 and Z_A depends on the calculations of the widths and the lengths of the sections. Section *A* and *B* are assumed to be quarter wave length transformers. The width of section A is considered as a given parameter. The length of section *A* can be determined by using Equation (5.6).

$$\text{length of section A} = (\lambda_g / 4) - d_A \tag{5.6}$$

Where λ_g is the wave length within the substrate and d_A is the shift of the minimum of the electric field from the aperture, corresponding to the discontinuity reactance [32] [33].

The wavelength λ_g can be determined by calculating the normal component of the electric field intensity below the conductor along y-axis in the middle of the

microstrip as it is known standing wave pattern (SWP), as illustrated by Figure 5.13. The FEKO simulated result of SWP for section A is shown in Figure 5.15.

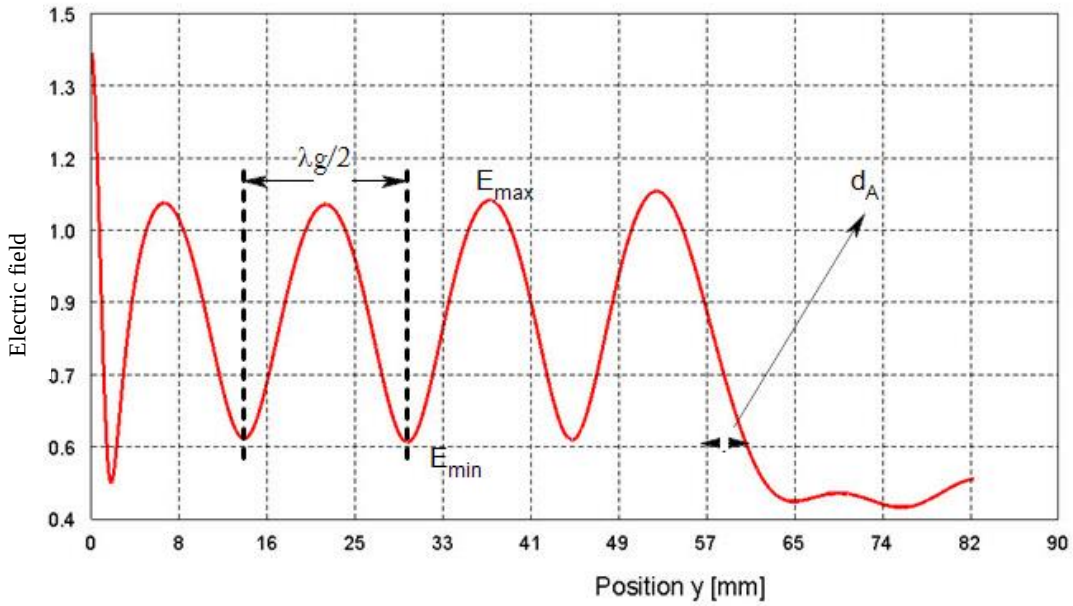

Figure 5.15: Standing wave pattern for section A (Aperture at 57.2mm)

The values determined from the SWP in Figure 5.15 (λ_g = 30.667 mm and d_A= 3.667 mm) are substituted in Equation (5.6) to calculate the length of the section A to be 4 mm. Section B width can be calculated by using the following Equations:

$$Z_B = \sqrt{Z_0 Z_R'} \tag{5.7}$$

$$Z_R' = Z_A \frac{1+|\Gamma|}{1-|\Gamma|} \tag{5.8}$$

$$|\Gamma| = \frac{E_{\max}}{E_{\min}} \tag{5.9}$$

Where: $|\Gamma|$ is the magnitude of the reflection coefficient.

The impedance of section B is evaluated to be 48.626Ω. The width of section B is determined by using the transmission line theory by applying Equations (4.10) and (4.11) given in Chapter 4. The value is evaluated to be 3.202 mm.

The length of section B can be calculated by the same method which was applied to section A length, by using Equation (5.8).

$$\text{length of section B} = (\lambda_g / 4) - d_B \qquad (5.8)$$

The SWP of the sections A and B was calculated to determine the variables in Equation (5.8) in order to calculate the length of section B as illustrated by Figure 5.16.

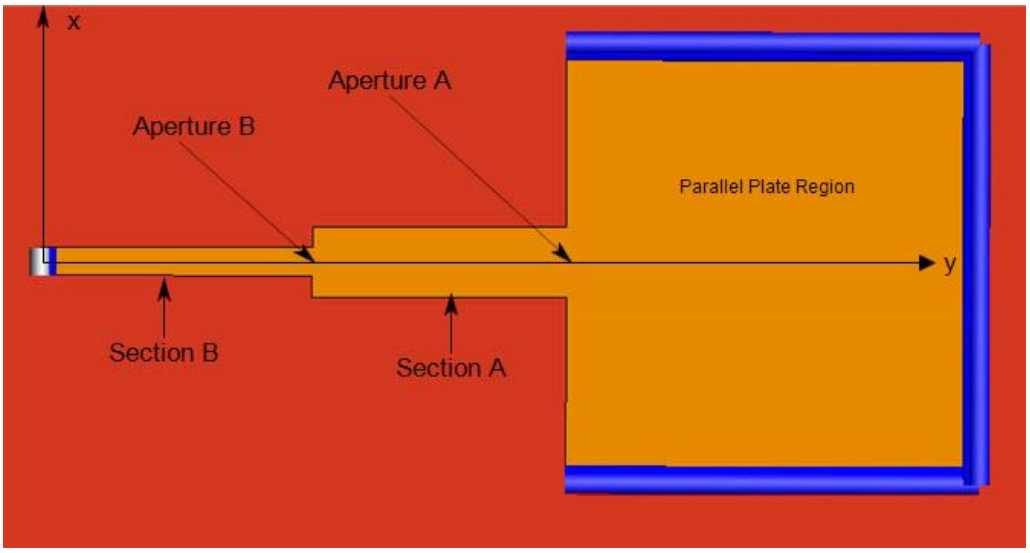

Figure 5.16: Transition between parallel plate and section B

The FEKO simulated result of SWP for the sections A and B is shown in Figure 5.17.

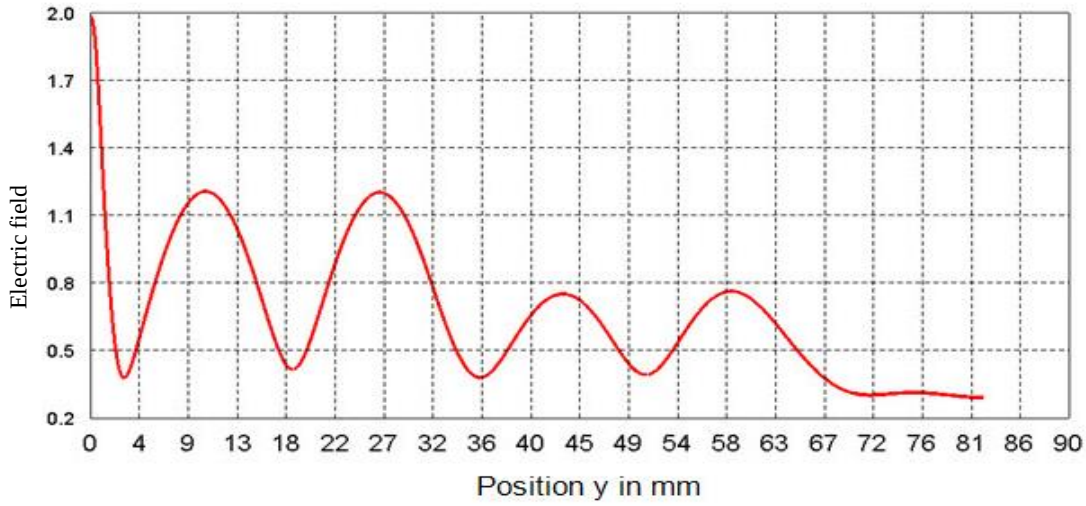

Figure 5.17: Standing wave pattern of section A and B

By substituting the values which is constructed from the simulated result in Figure 5.17 (λ_g = 32.884 mm and d_B = 2.63 mm) in Equation (5.8). The length of section B was estimated to be 5.591 mm.

After the estimation of the dimensions for sections A and B the following final geometry was shown in Figure 5.18 was obtained.

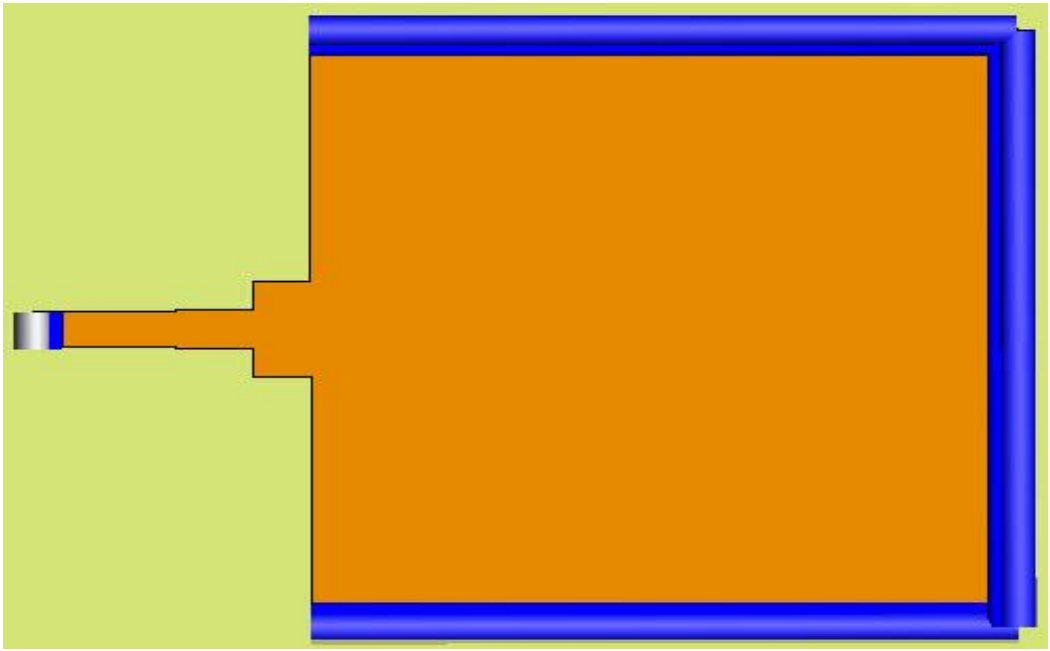

Figure 5.18: Section A and section B connected with parallel plate

The dimensions of all sections are described in Figure 5.19.

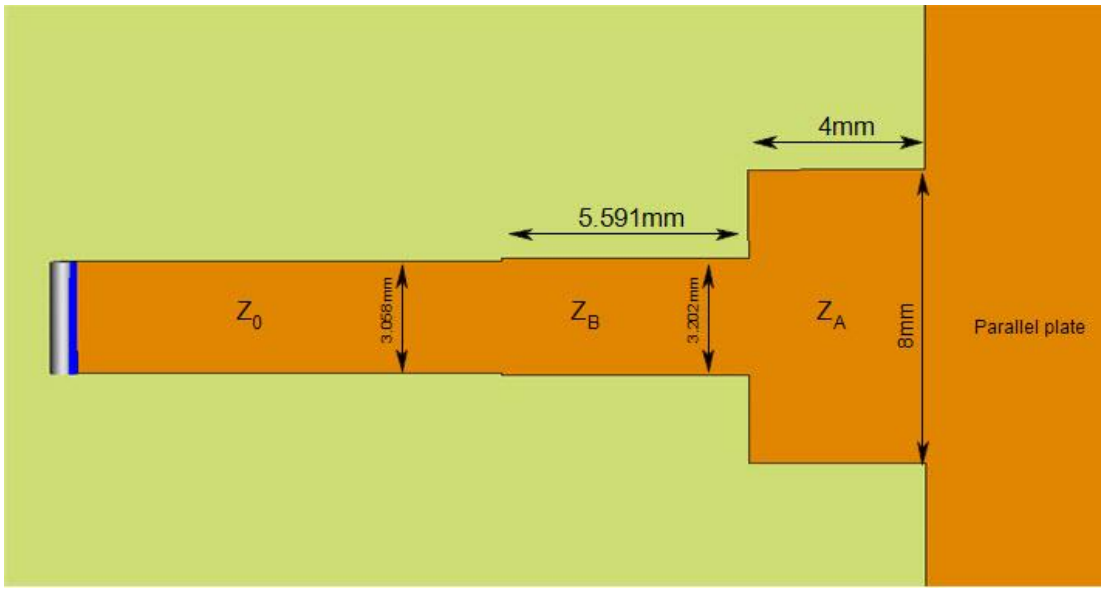

Figure 5.19: Dimensions of the multisession structure

Figure 5.20 shows the return loss for (4GHz-6GHz) bandwidth estimated by FEKO.

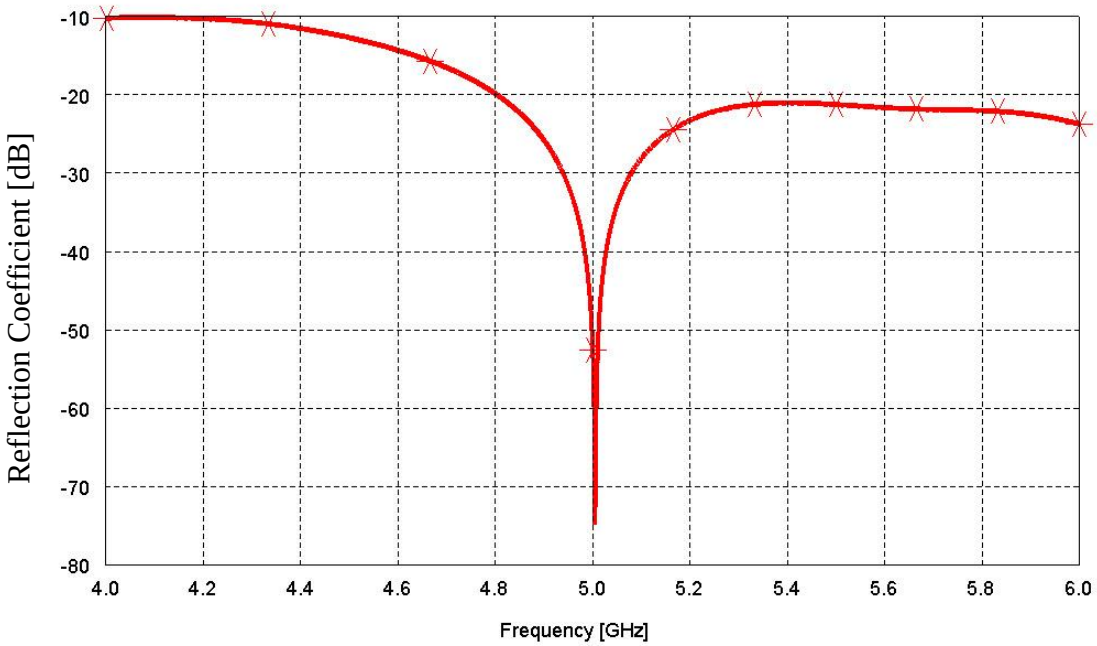

Figure 5.20: Reflection coefficient of the multi-sections taper

The simulation result indicates a good matching at the 5GHz for the multi section transition with zero return loss.

The parallel plate in the previous study was considered as a lens. This method will be applied to the lens geometry in the next sections.

5.4.2 Lens Matched with Transition Section

The lens geometry as it was explained has lower impedance than the transmission line due to its wide surface. In general used microstrip horn tapering technique is used to match the lens region to the feed line. But in this study a new transition technique is used for matching.

In this section, the method which was described in the previous section will be applied to the lens geometry for transition between the lens region and feed line. The lens design parameters are explained in Table 3.3. The aperture width for the centre port is 17.78 mm as shown in Figure 5.21.

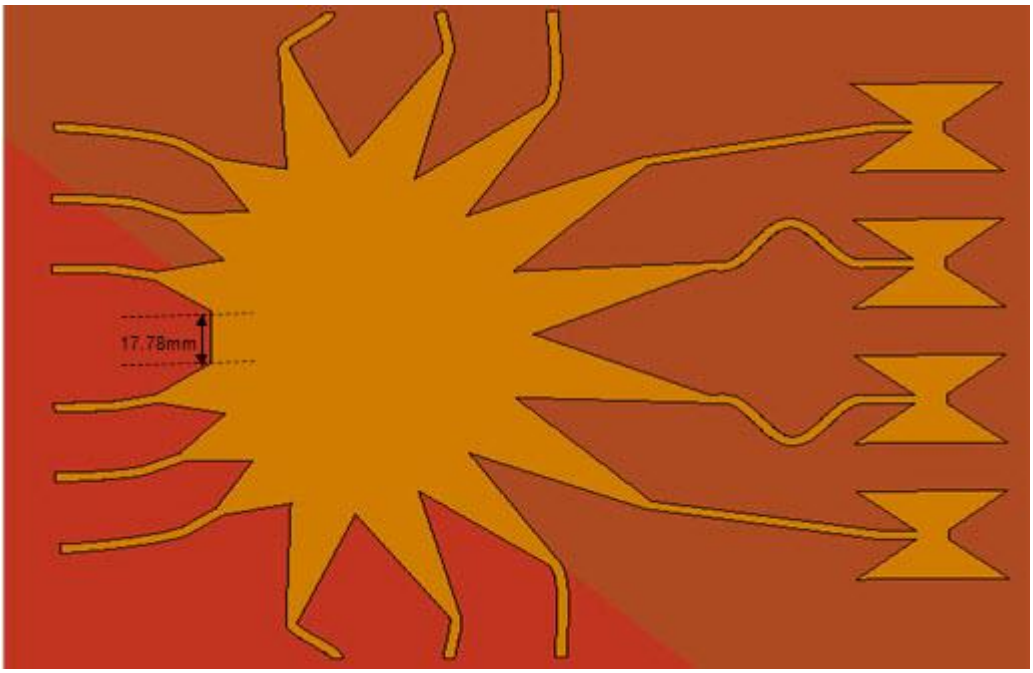

Figure 5.21: Centre port aperture

The length of section A can be calculated by using Equation (5.6). In order to calculate the near field of section A, the geometry given by Figure 5.22 is considered.

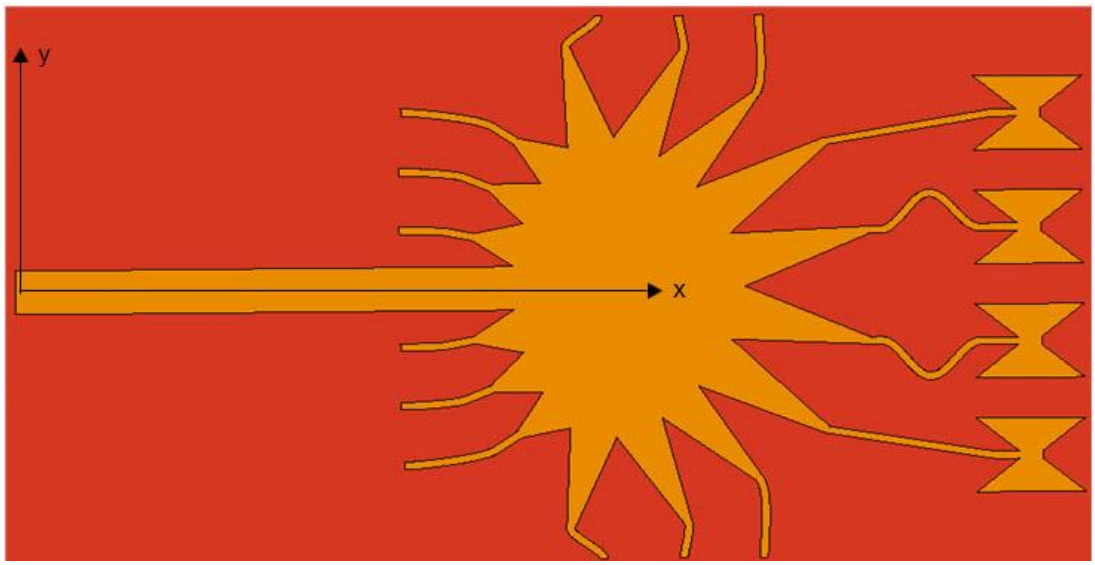

Figure 5.22: Lens with Section A

FEKO simulated result of the SWP for section A is shown in Figure 5.23.

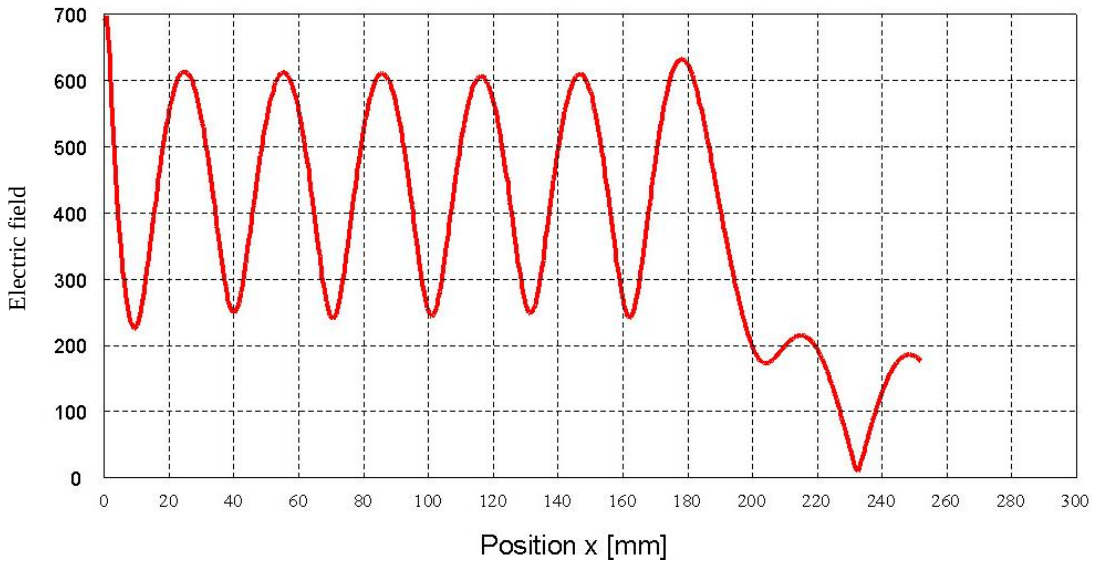

Figure 5.23: Standing wave pattern of Section A with connectedlens [Aperture at 186.228]

The estimated values of the wave length λ_g=61.45 mm and d_A=5.45 mm from the SWP result in Figure 5.23, by substituting these values in Equation (5.6) the length of section A calculated to be 9.91mm.

The width of section B is evaluated to be 4.66 mm by using Equations (5.7)-(5.9). To estimate the length of section B the near field below the sections A and B of the geometry shown in Figure 5.24 is considered.

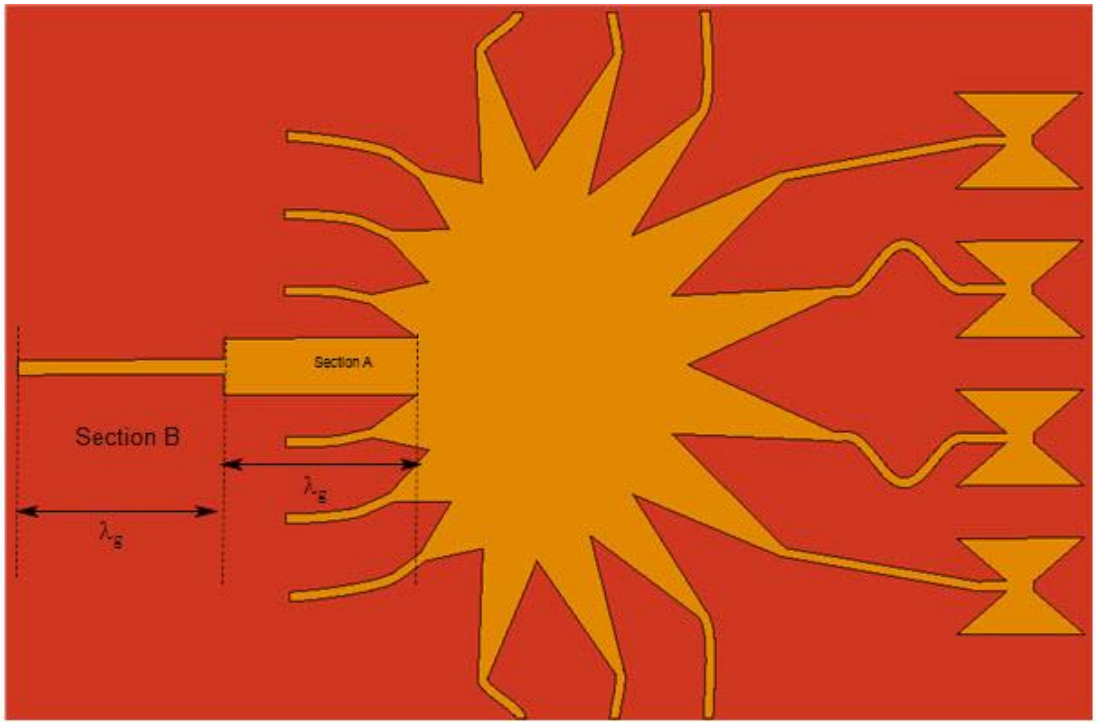

Figure 5.24: Sections A and B with the lens

The near field below in the center of the sections below the conductor simulated by FEKO is shown in Figure 4.25.

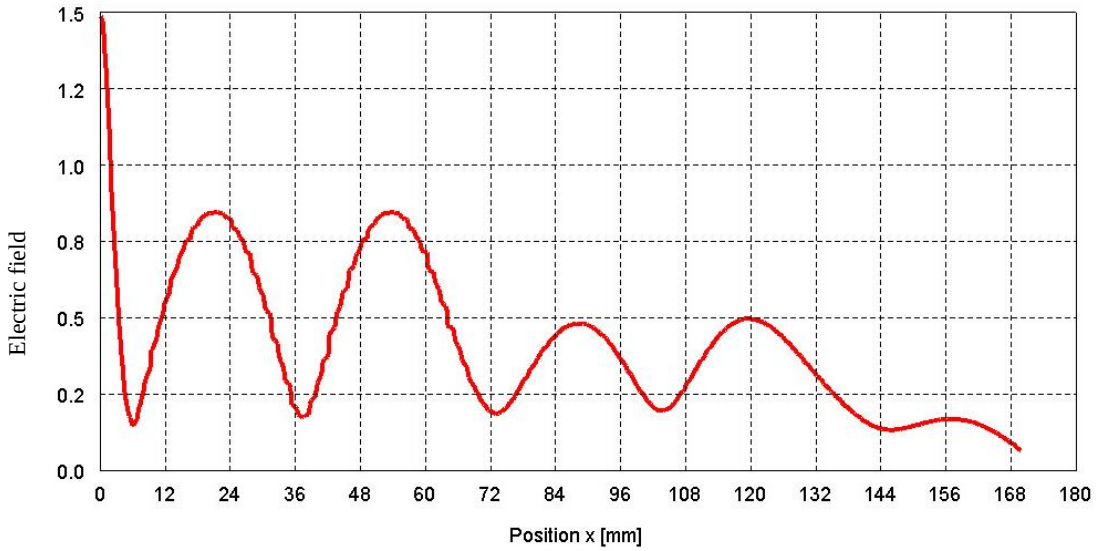

Figure 5.25: Standing wave pattern for section A and B [Apertures A at 128.057 and B at 65.981]

By substituting the variable obtained from the SWP result in Figure 5.25 (λ_g= 65.98 mm and d_B= 3.7 mm) in Equation (5.8), the length of section B is estimated to be 12.79 mm.

The final dimensions of sections A and B connected to the lens geometry are shown in Figure 5.26 and Figure 5.27.

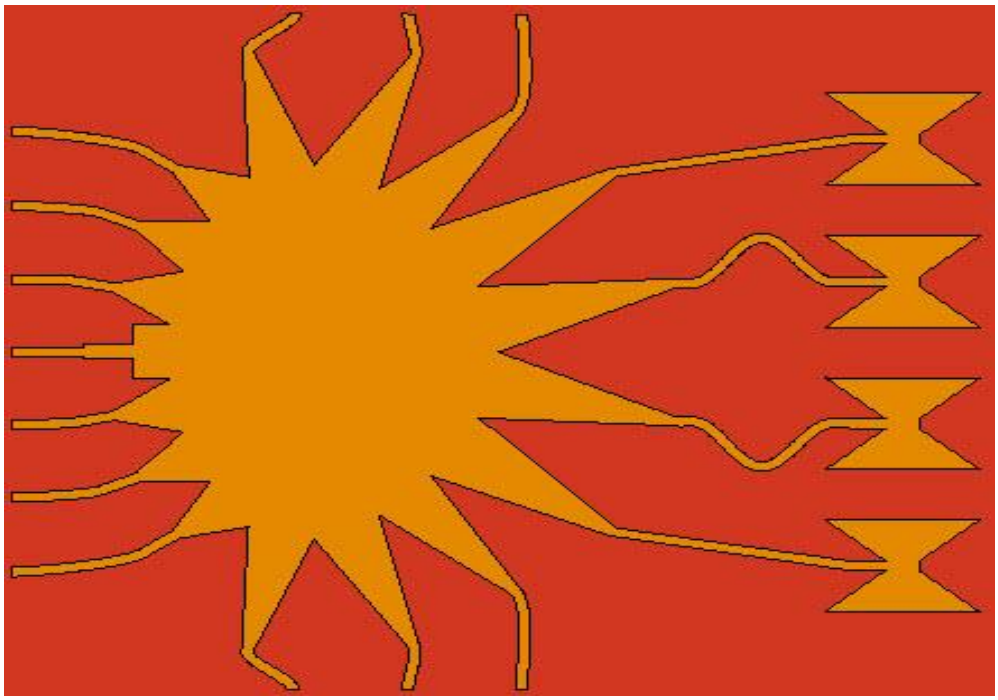

Figure 5.26: Lens with center port multi-section transition

Details of structure of sections A and B are explained in Figure 5.27.

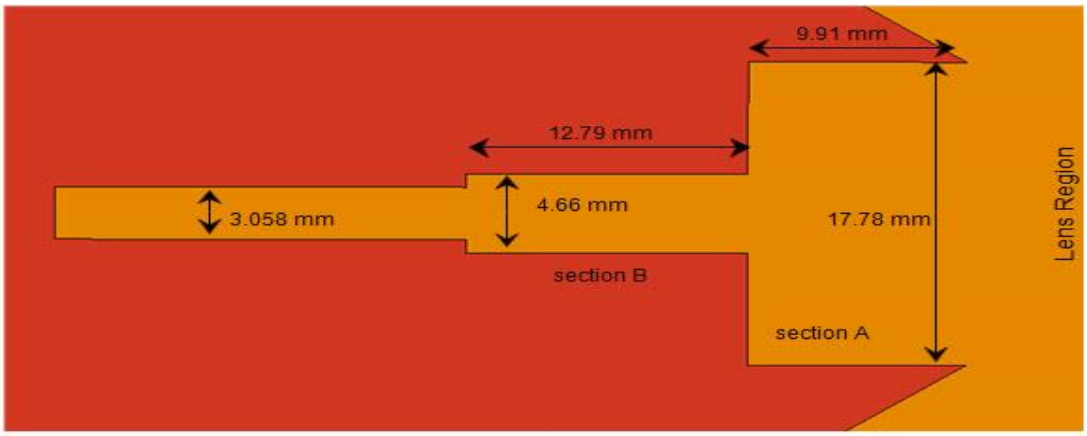

Figure 5.27: Description of the sections dimension for the center port

The return loss simulation result is shown in Figure 5.28, when the center port (with multi-section) was excited.

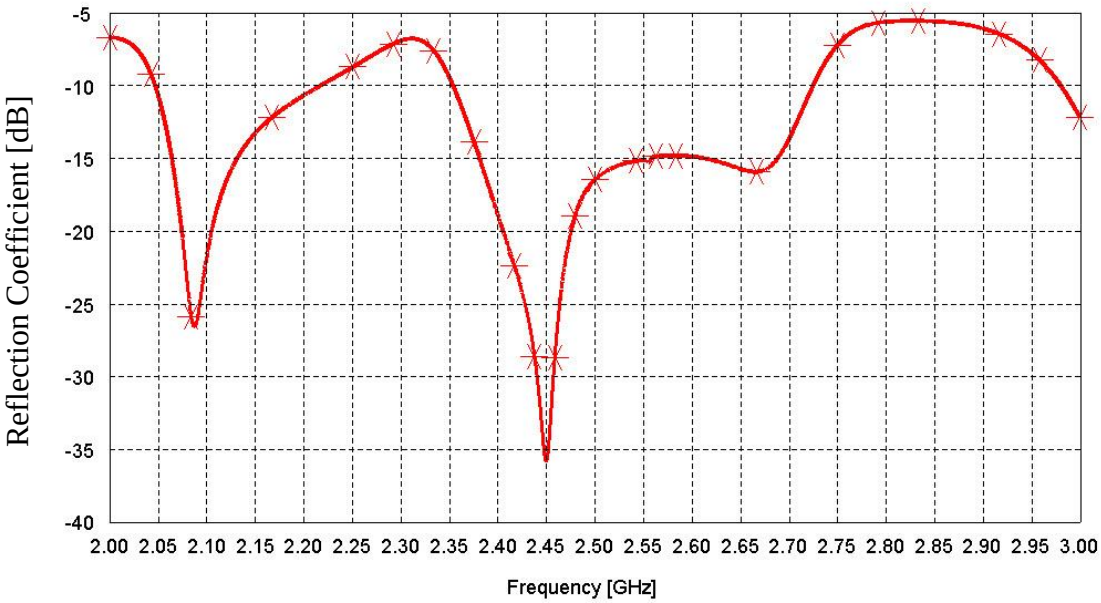

Figure 5.28: Reflection coefficient of multi-section port connected with lens

The result indicates an acceptable matching between the feed line and the lens region with reflection coefficient of about 0.01 at the design frequency 2.45GHz.

To compare between the horn taper and multisection transition Figure 5.29 shows the return loss of multisection transition and linear horn taper having the same length.

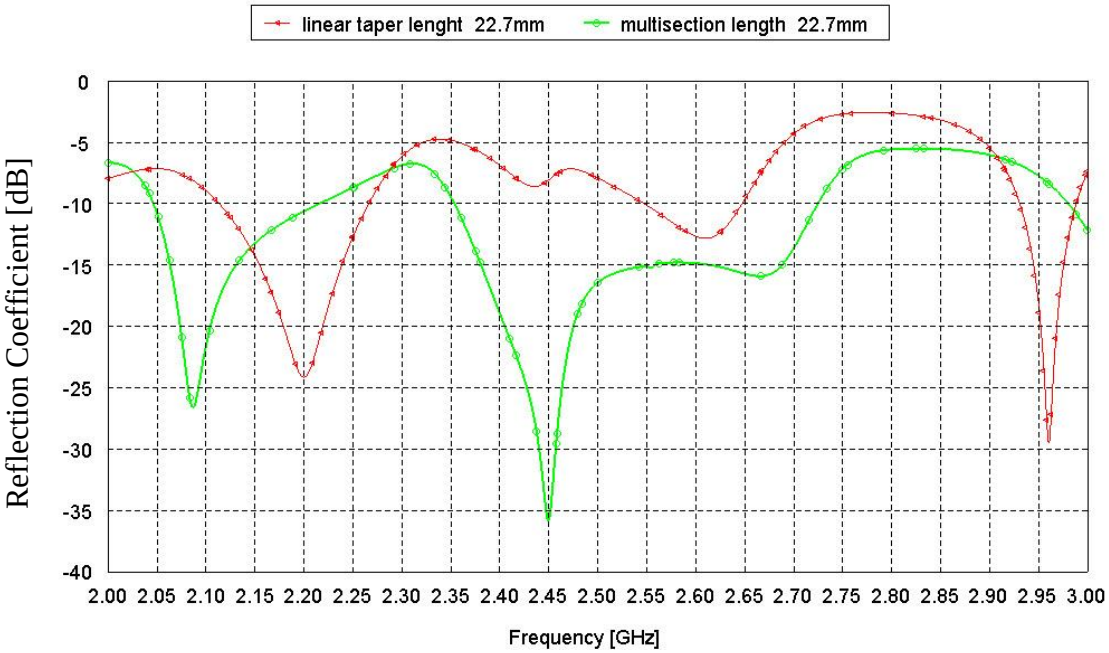

Figure 5.29: Comparison between multi-section transition and the horn linear taper

The results indicate the difference in the return loss for linear taper and multi-section transition with the same length. We can see that multisection design has minimum return loss at the deign frequancy.

The multi-section transition depends on the calculation of the standing wave pattern mainly. However, it is calculated in a shorter time compared with the linear taper. Also the minimum refelection can be achieved at the design frequancy.

Chapter 6

CONCLUSION AND FUTURE WORK

6.1 Conclusion

A beam direction changing has been applied by designing and simulating Rotman microstrip lens with seven beam ports and 2.45GHz center frequency connected to bowtie phased array antenna in this study.

The matching methods used to match between the lens region and the feeding line was designed and simulated by the implementations of horn taper.

A new matching technique between lens impedance and feeder impedance was developed and applied to the lens, by considering the lens as a parallel plate region with a certain width input aperture. This matching technique can be achieved with shorter time and less software platform complexity compared with other horn taper matching techniques.

6.2 Future work

Homogenous substrate region below the lens was considered in this study. The lens size and its performance can be improved with inhomogeneous medium. Lens side walls are used for reducing reflections, an optimization method can be developed to attain high performance side walls with short time. With wide development in communication system, design an adaptive steerable array antenna based on rotman

lens to be used in heterogeneous high speed, high energy efficiency, high bandwidth adopted with 5G cellar system can be considered very effective and practical idea.

REFERENCES

[1] W. Rotman, R. F. Turner, "Wide-Angle Microwave Lens for Line Source," *IEEE Transactions on Antennas and Propagation,* vol. 11, pp. 623-632, 1963.

[2] Junwei Dong, Rudolf Cheung, "A Computer Synthesized 2-8 GHz Printed Rotman Lens with 9x8 Input-to-Output Configuration," in *IEEE Antennas and Propagation Society International Symposium,* Spokane, WA, 2011.

[3] D. M. Pozar, Microwave Engineering, JohnWiley & Sons Inc., 2010.

[4] Richard C. Johnson, Antenna Engineering Hand Book, New York: McGraw-Hill, 1993.

[5] J. Blass, "The multidirectional antenna a new approach to stacked beams," *IRE International Convention Record,* vol. 8, pp. 48-50, 1966.

[6] J. McFarland, J. Ajioka, Beam-Forming Feeds, Van Nostrand Reinhold, 1993.

[7] Takashi Katagi, Seiji Mano, Shin-Ichi Sato, Seiichi Tahara, Eiji Tomimatsu, "An Improved Design Method Rotman Lens Antennas," *Antennas and Propagation,* vol. 20, pp. 136-139, 1982.

[8] Donald H. Archer, Michael J. Maybell, "Rotman lens development history at Raytheon Electronic Warfare Systems 1967-1995," in *Antennas and*

Propagation Society Internationa, 2005.

[9] C. A.Balanis, Antenna Theory, Canda: Wiley, 2005.

[10] H. J. Visser, Array and Phased Array Antenna Basics, The Atrium, Southern Gate, Chichester, England: Wiley, 2005.

[11] R. L. Haupt, Antenna Arrays, Canada: Wiley, 2010.

[12] J. Ruze, "Wide-Angle Metal-Plate Optics," *Proceedings of the IRE,* vol. 38, no. 1, pp. 53-59, 1950.

[13] J. E. Boyns, A. D. Munger, J. A. Provencher, J. Reindel, B. I. Small , "A Lens Feed for a Ring Array," *Antennas and Propagation,* vol. 16, no. 2, pp. 264 - 267, 1968.

[14] Shelton, J. Paul, "Focusing Characteristics of Symmetrically Configured Bootlace Lense," *Antennas and Propagation,* vol. 26, no. 4, pp. 513 - 518, 1978.

[15] R. M. Cox, J. R. Sebring , "MLS -A Practical Application of Microwave Technology," *Microwave Symposium,* pp. 322 - 324, 1976.

[16] R. C. Hansen, "Design trades for Rotman lenses," *Antennas and Propagation,* vol. 39, pp. 464 - 472, 1991.

[17] M. S. Smith, "Design considerations for ruze and rotman lenses," *Radio and Electronic Engineer,* vol. 52, pp. 181 - 187, 1982.

[18] M. S. Smith, A. K. S. Fong , "Amplitude performance of Ruze and Rotman lenses," *Radio and Electronic Engineer,* vol. 53, pp. 329 - 336, 1983.

[19] J. Rao, "Multifocal three-dimensional bootlace lenses," *Antennas and Propagation,* vol. 30, pp. 1050 - 1056, 1982.

[20] J. Dong, A. I. Zaghloul, Rotman R., "Phase error performance of multi focal and nonfocal two dimensional Rotman lens designs," *Microwaves, Antennas & Propagation, IET,* vol. 4, pp. 2097 - 2103, 2010.

[21] "Raytheon Company," June 2014. [Online]. Available: http://www.raytheon.com/.

[22] "The Federation of American Scientists (FAS)," June 2014. [Online]. Available: http://www.fas.org/.

[23] Yu Jian Cheng Wei Hong, Ke Wu, Zhen Qi Kuai, Chen Yu, Ji Xin Chen, Zhou, J.Y., Hong Jun Tang, "Substrate Integrated Waveguide (SIW) Rotman Lens and Its Ka-Band Multibeam Array Antenna Applications," *Antennas and Propagation,* vol. 56, pp. 2504 - 2513, 2008.

[24] Ozlem Kilic Steven J. Weiss, "Rotman Lens Applications for the US Army: A Review of History Present and Future," *Radio Science Bulletin,* vol. 333, pp. 10-21, 2010.

[25] "FEKO," EMSS, June 2014. [Online]. Available: http://www.feko.info/product-detail/overview-of-feko.

[26] Junwei Dong, A. I. Zaghloul, Rensheng Sun, C. J. Reddy, "EHF Rotman lens for electronic scanning antennas," in *Microwave Conference, 2008. APMC 2008. Asia-Pacific*, Macau, 2008.

[27] J. Dong, A. I. Zaghloul , "Phase-error performance of multi-focal and non-focal two-dimensional Rotman lens designs," *Microwaves, Antennas & Propagation, IET,* vol. 4, pp. 2097 - 2103, 2010.

[28] Leonard Halla, Hedley Hansenb, Derek Abbotta, "Rotman lens for mm-wavelengths," in *Centre for Biomedical Engineering and Department of Electrical and Electronic Engineering*, Australia.

[29] Ping-Chieh Chiang, Wen-Jiao Liao, Yun-Tsung Tu, Hsin-Chin Liu, "Implementation of direction-of-arrival estimation using Rotman lens array antenna," in *Hiroshima,* 2013.

[30] R. Uyguroglu, A. Y. Oztoprak , "A method for minimizing the phase errors of Rotman lenses," in *Electrical and Electronics Engineering, 2009. ELECO 2009.*

International Conference on, Bursa, 2009.

[31] J. S. Dahele, Kai Fong Lee, "On the resonant frequencies of the triangular patch antenna," *Antennas and Propagation, IEEE Transactions,* vol. 35, no. 1, pp. 100 - 101, 1987.

[32] R. Uyguroğlu and A. Y. Niazi, "Designing microstrip transitions into parallel-plate regions using the FDTD method," *Microwave and Optical Technology Letters,* vol. 22, p. 81–84, 1999.

[33] D. K. Cheng, Fundamentals of Engineering Electromagnetics, ADDISON WESLEY, 1993.